NASA
Technical
Paper
3046

1990

Prediction of Effects of Wing Contour Modifications on Low-Speed Maximum Lift and Transonic Performance for the EA-6B Aircraft

Dennis O. Allison
and E. G. Waggoner
Langley Research Center
Hampton, Virginia

National Aeronautics and
Space Administration
Office of Management
Scientific and Technical
Information Division

The use of trademarks or names of manufacturers in this report is for accurate reporting and does not constitute an official endorsement, either expressed or implied, of such products or manufacturers by the National Aeronautics and Space Administration.

Contents

Summary

Computational predictions of the effects of wing contour modifications on maximum lift and transonic performance were made and verified against low-speed and transonic wind-tunnel data. This effort was part of a program to improve the maneuvering capability of the Grumman EA-6B Prowler, an electronics countermeasures aircraft, which evolved from the A-6 Intruder, an attack aircraft. The predictions were based on results from three computer codes that include viscous effects: MCARF, a two-dimensional subsonic panel code; TAWFIVE, a transonic full-potential code; and WBPPW, a transonic, small-disturbance, potential-flow code. The modifications were previously designed with the aid of these and other codes. The wing modifications consist of contour changes to the leading-edge slats and trailing-edge flaps and were designed for increased maximum lift with minimum effect on transonic performance. This report presents the prediction of the effects of the modifications, with emphasis on verification through comparisons with wind-tunnel data from the National Transonic Facility. Attention is focused on increments in low-speed maximum lift and increments in transonic lift, pitching moment, and drag that result from the contour modifications.

The effects of the modifications on low-speed maximum lift coefficient were predicted two dimensionally and estimated three dimensionally at two Reynolds numbers. The estimates, based on results from MCARF, overpredicted the effect of the leading-edge modification but agreed well with experimental data for the effect of the trailing-edge modification. At the higher Reynolds number, the estimates and the experimental data showed a significant increase in the increment of maximum lift coefficient for the combined leading- and trailing-edge modification over that for the trailing-edge modification alone.

Effects of the modifications on transonic lift, pitching-moment, and drag coefficients were predicted by both the TAWFIVE and WBPPW codes. There was overall agreement between the experimental data and code results, in that the trailing-edge and combined modifications had more effect on the transonic characteristics than did the leading-edge modification. The relative effects of the modifications on transonic lift and pitching-moment coefficients were well predicted by both codes. The relative effects of the modifications on transonic drag coefficient were well predicted by the TAWFIVE code but poorly predicted by the WBPPW code.

Introduction

Langley Research Center has been involved in a cooperative program with the U.S. Navy and Grumman Aerospace Corporation to improve the maneuvering capability of the EA-6B Prowler (refs. 1 to 5). This cooperative program is one facet of the Navy's Advanced Capability Program (ADVCAP) for the EA-6B, an electronics countermeasures aircraft that evolved from the A-6 Intruder, an attack aircraft. The EA-6B is a four-place, twin-engine configuration with a midfuselage-mounted wing. The wing is swept back 25.5° at the quarter-chord and has an aspect ratio of 5.31. Wing contours are based on the NACA 64-series airfoils. The EA-6B and the A-6 configurations are different in that the EA-6B has an extended fuselage, a pod-shaped fairing on top of the vertical tail, and an engine with approximately 20 percent more sea-level thrust. However, the planforms, section contours, and aerodynamics of the wings for the two aircraft are similar. One of the most obvious differences between the two aircraft is the weight. The A-6 has a maximum landing weight of 36 000 lb, and the EA-6B has a maximum landing weight of 45 500 lb. This weight increase, coupled with virtually the same wing characteristics, results in significantly reduced stall maneuver margins. For example, in a $2g$ (60° banked) turn at 250 knots, the margin above stall speed is reduced by about 50 percent for the EA-6B relative to the A-6.

One objective of the maneuver-improvement program was to improve the low-speed high-lift capability of the EA-6B by designing relatively simple wing modifications that would not degrade high-speed cruise performance. To avoid major modifications that may involve changes to the wing box, the wing modifications were constrained to contour changes of the leading-edge slat and trailing-edge flap. The effort focused on computational design and experimental verification of the wing-section modifications. A variety of two- and three-dimensional low-speed and transonic computational techniques were used during the design effort. Modifications were defined that yielded significantly increased maximum lift at low speed with minimal impact on high-speed cruise performance. The results were verified experimentally during extensive two-dimensional (2D) and three-dimensional (3D) testing in several wind tunnels at Langley Research Center.

This report presents the prediction of the effects of leading- and trailing-edge contour modifications, with particular emphasis on verification through comparisons with experimental data. Often, the experimental data were available at conditions that differed slightly from those used in the

computational design effort. Code results were subsequently generated to verify the prediction of incremental effects of the modifications at conditions that matched those of selected experimental data. Selected experimental data (refs. 2 and 3) were used from 2D testing in the Langley Low-Turbulence Pressure Tunnel (LTPT) and from 3D testing in the National Transonic Facility (NTF). The NTF test included a wing-body configuration with no stores, tail, or external antennas modeled but with various combinations of baseline and modified slats and flaps.

Attention was focused on increments in low-speed maximum lift and increments in transonic lift, pitching moment, and drag resulting from the contour modifications. No low-speed computational method was available for the prediction of maximum lift coefficient in three dimensions to compare with data from the NTF test. Nevertheless, increments in 3D maximum lift coefficient were estimated with a 2D subsonic code and the application of simple sweep theory. These estimated increments were compared with corresponding low-speed data from the NTF test. Two transonic potential-flow computational methods capable of modeling wing-body configurations were applied. Results from these two codes were compared directly with transonic data from the NTF test.

This report describes the prediction and verification effort in detail. Included are descriptions of the computational methods used, the configuration and wing modifications, and the manner in which the codes were applied. The multiple-design-point philosophy used when the modifications were designed can be inferred. Results with verification consist of comparisons between the computational predictions and data from both two- and three-dimensional experiments.

Symbols

C_D	wing-body drag coefficient
C_L	wing-body lift coefficient
C_M	wing-body pitching-moment coefficient
c	local chord
c_l	section lift coefficient
g	acceleration due to gravity ($1g = 32.2$ ft/sec^2)
M	Mach number
R	Reynolds number based on chord
t	airfoil thickness
x	streamwise coordinate
y	vertical coordinate
α	angle of attack
η	spanwise location (see fig. 2)
Λ	quarter-chord sweep angle

Subscripts:

l	lower surface
max	maximum
u	upper surface

Abbreviations:

bl	baseline (no modification)
LTPT	Langley Low-Turbulence Pressure Tunnel
le	leading-edge modification
MCARF	two-dimensional subsonic panel code
NTF	National Transonic Facility
TAWFIVE	transonic full-potential code
Te	thick trailing-edge modification
te	thin trailing-edge modification
WBPPW	transonic, small-disturbance, potential-flow code
2D	two dimensional
3D	three dimensional

Computations

Computations were made to predict incremental effects of wing contour modifications on low-speed maximum lift coefficient and transonic lift, pitching-moment, and drag coefficients for a wing-body configuration. The computational methods, the configuration, including modifications, and the application of the codes to that configuration are described in the sections that follow.

Computational Methods

One 2D subsonic and two 3D transonic computational methods were used to predict aerodynamic force and moment coefficients. A brief description of each computer code is given, and all three include viscous effects.

MCARF code. The multi-component airfoil code, MCARF (refs. 6 and 7), is a two-dimensional subsonic panel code. The inviscid solution is found by using a distributed vortex concept to solve the

Laplace equation. Compressibility effects are represented through the use of the Karman-Tsien correction. Viscous effects are included by iteratively updating the airfoil shape to include the displacement thickness from both laminar and turbulent boundary-layer calculations. A laminar boundary layer is calculated by using the basic approach of Cohen and Reshotko (ref. 8). The Schlichting-Ulrich-Granville method (refs. 9 and 10) is used to predict laminar instability and the subsequent transition location. The method of reference 11 is used to predict laminar stall. The turbulent boundary-layer thickness and turbulent stall are computed by using integral techniques.

TAWFIVE code. The computer code for transonic analysis of a wing and fuselage with interacted viscous effects, TAWFIVE (ref. 12), uses the interaction of an inviscid and a viscous flow solver to obtain transonic flow-field solutions about wing-fuselage combinations. The inviscid flow field is solved by using a conservative, finite-volume, full-potential method based on FLO-30 by Caughey and Jameson (ref. 13). No modifications were made to the internal grid-generation algorithm in FLO-30, which uses a body-fitted, sheared, parabolic coordinate system. Viscous and wake curvature effects were added to the FLO-30 code to formulate the TAWFIVE code. Viscous effects are computed by using a three-dimensional compressible integral method capable of computing laminar or turbulent boundary layers with a fixed transition location. The laminar technique is that developed by Stock (ref. 14), and the turbulent method is based on the work of Smith (ref. 15) with extensions (ref. 16). An important feature of the code is Streett's treatment of the wake (ref. 17). The wake model used in FLO-30 was replaced with a model which includes effects resulting from the thickness and curvature of the wake in the solution. These effects can make significant differences in results obtained on various configurations (ref. 17).

WBPPW code. The wing-body-pod-pylon-winglet code, WBPPW, developed by Boppe (ref. 18) has been validated for many configurations (e.g., ref. 19). The code solves for the flow field at transonic speeds about a wing-fuselage configuration that can include engine pods or stores, wing pylons, and winglets. Using finite-difference approximations, a modified small-disturbance potential-flow equation is iteratively solved in a system of multiple embedded grids. The modifications to the classical small-disturbance equation provide more accurate resolution of shock waves with large sweep angles and a better approximation of the velocity where the flow equation changes type. Viscous effects are incorporated into the solution by the addition of boundary-layer displacement slopes to the wing-surface slopes. This in effect provides an equivalent "fluid" wing shape for analysis by the potential flow solver. The WBPPW code is capable of computing laminar or turbulent boundary layers with a fixed transition location. Boundary-layer displacement thickness for slope determination is computed from a modified Bradshaw turbulent method (ref. 20) and from the Thwaites laminar method modified for compressible flow. These two methods are extended to include sweep effects by using a procedure developed by Mason (ref. 21).

Configuration To be Modeled

The codes described previously were applied to a wing-body configuration that was tested in the NTF (ref. 3) and for which streamwise airfoil sections were tested in the LTPT (ref. 2). The full-scale configuration had a wing span of 53.0 ft, an aspect ratio of 5.31, and a quarter-chord sweep of 25.5°. (A planform sketch is shown in fig. 1.) The NTF test involved configurations that consisted of only the fuselage and wing, as well as those that included horizontal and vertical tails, up to seven stores, and/or an antenna under the fuselage. The three-dimensional configuration for which computational analyses were performed consisted of only the fuselage and wing with slats and flaps in the cruise configuration (i.e., no slat or flap deflection). The configuration modifications consisted of contour changes to the leading-edge slats and trailing-edge flaps. These modifications were designed (ref. 3) at the inboard and outboard design stations indicated in figure 1. The sketch of the wing presented in figure 2 indicates the spanwise extent of the slats and flaps. The shape of the root region used for computational modeling is also shown in figure 2.

The modifications were confined to the slats and flaps, except that on the lower surface the trailing-edge modifications began at $x/c = 0.70$ and the flap began at $x/c = 0.82$. There were two trailing-edge modifications: each had more camber and a thicker base than the baseline configuration. They are referred to as the thick (Te) and thin (te) trailing-edge modifications and had base thicknesses of approximately $0.011c$ and $0.006c$, respectively. Both were tested two dimensionally in the LTPT. However, only the thin trailing-edge modification was tested in the NTF. There was one modified leading edge (le), and it was more blunt than the baseline configuration and slightly drooped at the outboard station. Baseline (bl) and modified streamwise airfoils are given for

the inboard design station ($\eta = 0.28$) in figure 3 and table I and for the outboard design station ($\eta = 0.75$) in figure 4 and table II. The modifications at other stations were determined by linear interpolation or extrapolation of dimensional airfoil coordinates.

Computational Procedures

The application procedures used with each of the three computational codes are discussed without results in the sections that follow. Some of the experience gained during the use of each code is described. (The importance of user experience is discussed in reference 19.) For high-lift predictions, the 2D subsonic code was used because no prediction method was available for 3D low-speed maximum lift coefficient. The 3D transonic codes were used for predictions of lift, pitching moment, and drag coefficients.

MCARF application. Increments in 3D low-speed maximum lift coefficient were estimated through integration of increments in section coefficients that were determined with the 2D code, MCARF (refs. 6 and 7), and application of simple sweep theory. The code was used to predict 2D maximum lift coefficients at the inboard and outboard design stations with transition strip positions specified.

Transition strip locations for both the upper and lower surfaces were specified at the experimental positions. The code, however, predicted whether transition occurred before, at, or after a strip location. Upper surface transition was often predicted at the suction peak near the leading edge upstream of the strip location. Lower surface transition was predicted downstream of the strip location when the transition Reynolds number was too low (below 100).

Three maximum lift or stall criteria were monitored in the output from the MCARF code. Two of the criteria were concerned with leading-edge separation, and the third was concerned with trailing-edge separation. The first criterion was that the airfoil stalled when the local Mach number was greater than 1.0 at the point of laminar boundary-layer separation. The second criterion was an empirically determined one (ref. 11) based on the Morgan laminar stall parameter, PARB. Based on the recommendation in reference 11, if PARB exceeded 725, it was assumed there was no turbulent boundary-layer reattachment and the airfoil stalled. The final criterion concerned turbulent boundary-layer separation from the trailing edge; stall was considered to occur if turbulent separation occurred ahead of 90 percent chord. The airfoils were analyzed at angle-of-attack increments of 0.1°, and the three stall criteria were monitored. The maximum lift coefficient was assumed to be the lift coefficient at the highest angle of attack prior to stall.

Simple sweep theory was applied to convert 3D experimental conditions to 2D code inputs and to convert 2D code results to 3D results. The quarter-chord sweep angle of 25.5° was used in the conversions. Mach number and Reynolds number were converted to 2D conditions by factors of $\cos \Lambda$ and $\cos^2 \Lambda$, respectively. Analysis Reynolds numbers were also adjusted to account for the local chord at the inboard or outboard station. Maximum lift coefficients at each station were computed from the 2D code and were converted by the $\cos^2 \Lambda$ factor to get 3D section maximum lift coefficients. Each modified-section coefficient was subtracted from the corresponding baseline-section coefficient to obtain a 3D modified-section maximum-lift-coefficient increment.

Predicted increments in inboard and outboard 3D section coefficient were integrated by using the trapezoidal rule to yield a predicted increment in maximum lift coefficient for each modified wing configuration. The integration was over the region of the wing at which both the slat and flap were present from $\eta = 0.25$ to 0.85 (fig. 2). An assumption was made that the incremental maximum lift coefficients for the sections at $\eta = 0.25$ and 0.85 were equal to those for the inboard and outboard design stations at $\eta = 0.28$ and 0.75, respectively.

TAWFIVE application. Transonic lift, pitching-moment, and drag coefficients were predicted by using the TAWFIVE code (ref. 12). Initially, inviscid calculations were made for the baseline configuration without considering the glove inboard of $\eta = 0.25$. Effects of geometry modeling, viscosity, and convergence strategy were then explored to arrive at the final results.

The configuration was modeled by specifying a series of airfoil sections for the wing and a series of fuselage cross sections for the body. There was no explicit control of the intersection of the wing and body available to the user. When a detailed body shape was tried, problems with the computational grid in the region of the wing-body junction resulted in unrealistic wing boundary-layer separation and consequent termination of the computation. Subsequently, an axisymmetric body shape was tried with a linear variation of radius in the region near the wing and with an area distribution that approximated that of the detailed body. This axisymmetric shape worked successfully and was acceptable, since details of the body shape were not important in the determination of the effects of the wing contour modifications. Also, both this axisymmetric body and the detailed shape used in the WBPPW code are models

of the A-6 fuselage, which is shorter than that of the EA-6B (ref. 5). A planform sketch of the TAWFIVE computational wing-body configuration is shown in figure 5(a), and the input wing planform is shown in figure 2. The TAWFIVE code requires the wing root to lie outside the body and extends the inboard region of the wing to establish the wing-body juncture. The leading edge of the inboard region of the wing from $\eta = 0.19$ to 0.20 was originally turned perpendicular to the body centerline and was finally swept 30° (see fig. 2) to minimize unreasonable pressure variations at the wing root. Also, each spanwise end of the modified (slat and flap) region was modeled by specifying modified and baseline airfoils separated by less than 0.01 percent of span. Both the leading- and trailing-edge modifications were modeled from $\eta = 0.25$ to 0.88. The ends of the actual slats and flaps were at slightly different locations, as seen in figure 2.

Viscous effects were added in stages by running the TAWFIVE code in the inviscid mode, including viscosity on the wing, including the wake effect, and varying the number of viscous iterations. Also, computations were run at flight Reynolds numbers and later at tunnel Reynolds numbers, where boundary-layer separation was more of a problem. Boundary-layer calculations would sometimes terminate program execution as a result of unreasonable pressure variations at the wing root and tip. Some relief from this problem was found by altering the procedure used for the root and tip boundary-layer calculations. In the altered procedure, the root boundary layer was computed by using the pressure distribution from the next spanwise station, and the tip boundary layer was computed by using the pressure distribution from the previous spanwise station.

Convergence strategy for the TAWFIVE code involved choices of the number of inviscid iterations, initial values for potential and boundary-layer quantities, and a boundary-layer underrelaxation parameter. Various strategies were tried, which were intended to monotonically increase (rather than overshoot) lift and to avoid successively attached and separated boundary layers. Based on the criteria of minimized lift overshoot and consistent boundary-layer separation, the following strategy was chosen for generation of the results in this paper. The initial numbers of inviscid iterations on the coarse, medium, and fine grids were 30, 20, and 10, respectively, and then the first boundary layer was calculated. The second set of inviscid iterations started with the potentials set to zero, but with the previously determined boundary-layer correction on the wing and wake (without wake curvature effects) and with 60, 40, and 20 inviscid iterations on the coarse, medium, and fine grids, respectively. After each set of inviscid iterations, the boundary layer was updated. Each of the 3rd through 10th sets consisted of 50 inviscid iterations on the fine grid and used previous values of potential and boundary-layer quantities, including wake curvature effects. The relaxation parameter was specified at 0.6 for all boundary layers. Results were printed and plotted after the 4th, 7th, and 10th sets of iterations to monitor convergence.

WBPPW application. The WBPPW code (ref. 18) was also used to predict transonic lift, pitching-moment, and drag coefficients. Initially, runs were made that utilized the embedded body grid and relatively few inviscid and viscous iterations. Then geometric, viscous, and convergence effects were considered before the final results were computed.

Wing-body geometry was modeled by specifying a series of airfoil sections for the wing and by using the Quick-Geometry System (ref. 22), which provides a continuous analytical model of the fuselage. The portion of the wing from $\eta = 0.20$ to 0.25 in figure 2 (disregarding $\eta = 0.19$ to 0.20) was projected to the centerline to form the root. The code determined the intersection of the wing with the fuselage. Figure 5(b) is a planform sketch of the computational wing body. The transonic wing-thickness scaling factor was disabled in the code. The fine (embedded) wing grid was positioned with equal portions above and below the wing. The fine body grid was not utilized because it was assumed that the choice of body grid would have little influence on the incremental effects of the wing contour modifications. The leading- and trailing-edge modifications were specified between $\eta = 0.25$ and 0.88 in exactly the same way as they were for the TAWFIVE code.

Viscous effects were computed with very few boundary-layer updates in the earliest runs of the WBPPW code. Additional iterations were used to achieve convergence as described subsequently in this section. The value of 0.6 was used for the boundary-layer relaxation factor. Flight Reynolds numbers were specified for the first few runs, followed by wind-tunnel Reynolds numbers, which were specified for all the final runs.

The results in this paper have been corrected for a body-pressure drag error and a body-friction drag error in the WBPPW code. The body-pressure drag error was in equation (60) of reference 22, which should have a minus sign in front of both terms (the same error exists for pod-pressure drag in equation (39) of reference 18). The body-friction drag error in the code arose from the use of Reynolds number based on wing mean aerodynamic chord, where

Reynolds number based on body length should have been used as shown in equation (64) of reference 22. The first correction (which simply caused the body-pressure drag to change sign) increased the drag coefficient by amounts from 0.0048 to 0.0106. The second correction decreased the body-friction drag coefficient by 0.0016. The net effect was that the total drag coefficient increased by amounts from 0.0032 to 0.0090 for the WBPPW cases in this report.

Convergence strategy for the WBPPW code was formulated in terms of the numbers of inviscid crude- and fine-grid iterations and the number of fine-grid iterations for which the boundary layer was updated after every 20 iterations. There was a tendency for the lift, which was consistently low, to continue to grow throughout the iterations. The chosen strategy involved a sufficient number of inviscid iterations to quickly bring the lift up close to a converged level. The final results were computed by using a strategy in which 300 crude and 100 fine inviscid iterations were performed, followed by 400 fine iterations for which the boundary layer was updated 20 times. To monitor convergence, printed and plotted output was obtained after the inviscid iterations and after 10 and 20 boundary-layer updates.

Results and Verification

Computational results were generated by the application of codes as described previously. Comparisons with LTPT and NTF data at low-speed high-lift conditions are presented, followed by comparisons with NTF data at transonic cruise conditions. Emphasis is placed on incremental results, and the increment is always from the baseline to a modified configuration.

Comparisons with LTPT data were made to verify the 2D computations. However, the set of modifications tested in the LTPT entry (ref. 2) did not include the leading-edge modification alone (le) or the thin trailing-edge modification alone (te). The modifications that were chosen from the LTPT test for comparisons in this paper are: the thick trailing-edge modification alone (Te), the combined leading-edge and thick trailing-edge modification (le and Te), and the combined leading-edge and thin trailing-edge modification (le and te).

Most of the results in this paper are compared with NTF data. The NTF data consist of those published in reference 3 plus unpublished data from the same test. The modifications tested in the NTF were for the leading edge alone, the thin trailing edge alone, and for these two combined. Comparisons between computational results and NTF data were made for these modifications.

Low-Speed Maximum Lift

Computational estimates were made of increments in maximum lift coefficient between the baseline and modified wing-body configurations, which were tested in the NTF at $M = 0.3$ and $R = 1.4$ and 5.4×10^6. Estimates of increments in 3D maximum lift coefficients were made (as explained in the section *MCARF application*) from 2D computations with application of simple sweep theory. To verify the 2D computations, results from the MCARF code were first compared with corresponding 2D data from the LTPT; 3D estimates were then compared with the NTF wing-body data.

MCARF results, LTPT data. Two-dimensional comparisons were made between MCARF code results and corresponding LTPT data for contour modifications and Mach number closely related to those in the NTF test. The LTPT data (ref. 2) for the baseline and modified airfoils are presented in figure 6 for a range of Mach numbers. The following observations can be made from figure 6 for the airfoil modifications at a Reynolds number of 10×10^6. First, the thick trailing-edge modification produced a significant gain in maximum lift coefficient. Second, in combination with Te, the leading-edge modification produced a significant additional benefit. Third, in combination with le, the thin trailing-edge modification produced about the same benefit as Te. Fourth, the benefits of all the modifications were sensitive to compressibility effects and, in general, decreased with increasing Mach number. Figure 6 consists of 2D data for configurations closely related to those in the NTF test; a 2D Mach number is still needed. The low-speed data were taken in the NTF at $M = 0.3$, and the model sweep angle was 25.5°. The corresponding 2D Mach number is $M \cos \Lambda = 0.271$.

Comparisons were made (fig. 7) between the LTPT maximum lift coefficients and those predicted from the MCARF computations at $M = 0.271$ and $R = 10 \times 10^6$. The transition strip location was modeled in the code at the LTPT positions of $x/c = 0.150$ on the upper surface and $x/c = 0.050$ on the lower surface. The code predicted that upper surface transition occurred at the suction peak (before the strip location) and lower surface transition occurred at the strip location of $x/c = 0.050$, with one exception. Lower surface transition was predicted to be at $x/c = 0.770$ on the airfoil with the combined leading-edge and thick trailing-edge modification. For all four airfoils, the stall criterion met was that the local Mach number exceed unity at the point of laminar boundary-layer separation.

The computed data for maximum lift coefficient qualitatively followed the trend of the LTPT data and were about 5 to 10 percent low. (See fig. 7(a).) The computed increment (from the baseline to each modified configuration) in maximum lift coefficient also followed the trend of the LTPT data and was about 30 percent low. (See fig. 7(b).) Both the predictions and the LTPT data showed that the combined modification yielded about three times the benefit of the trailing-edge modification alone and that the two trailing-edge modifications were equally effective when combined with the leading-edge modification.

Estimated results, NTF data. Comparisons were made between estimated increments in 3D maximum lift coefficients and those from the NTF test at $M = 0.3$ and $R = 1.4$ and 5.4×10^6. Experimental increments in maximum lift coefficient for the three modifications were obtained by using data (fig. 8) from the NTF test (ref. 3). For the estimates, the MCARF code was applied with the transition strip locations (from the NTF test) on the upper and lower surfaces at $x/c = 0.043$ for the inboard station and $x/c = 0.073$ for the outboard station. For the cases in this paper, the code predicted that upper surface transition always occurred near the leading edge at the suction peak. Lower surface transition was predicted after the strip location, between $x/c = 0.98$ and 1.00 without the trailing-edge modification and between $x/c = 0.74$ and 0.78 with the trailing-edge modification. The only exception was for the outboard station at $R = 5.4 \times 10^6$, where lower surface transition was predicted at the strip location ($x/c = 0.073$) for the baseline configuration and all three modified configurations. The stall criterion that the local Mach number exceed unity at the point of laminar separation was met in all cases. A peculiar boundary-layer separation that the MCARF code predicted for the outboard station without the leading-edge modification at $R = 1.4 \times 10^6$ was disregarded. This upper surface separation did not come forward from the trailing edge, it simply appeared in the turbulent boundary layer behind a laminar bubble at $x/c \approx 0.004$ as the stall angle was approached. This predicted separation was considered to be nonphysical. Estimated increments that were computed considering this phenomenon an additional stall criterion were not significantly different from those given in this paper.

Estimated increments in 3D maximum lift coefficient are compared with the NTF data increments in figure 9. The estimated increments do not change significantly with Reynolds number, but the measured increments do change. This suggests that the Reynolds number effect that occurs three dimensionally may not occur two dimensionally (the estimates are based on predictions from a 2D code). The effects of the leading-edge modification are highly overestimated, but the estimates for the trailing-edge modification agree well with the NTF data. The increment for the combined leading- and trailing-edge modification is overestimated, but it is in better agreement at the higher Reynolds number (fig. 9(b)). At the higher Reynolds number, which more closely represents flight conditions, the estimates and NTF data both show a very significant increase in the increment for the combined modification over that for the trailing-edge modification alone.

Transonic Performance

Lift, pitching-moment, and drag coefficients were computed by using the TAWFIVE and WBPPW codes for comparison with NTF data. Analyses were conducted at Mach and Reynolds numbers that match the experimental data. The four (baseline plus three modified) configurations were analyzed for the cruise design condition of $M = 0.800$ and $\alpha = 2.5°$ ($C_L \approx 0.3$) and for a lower speed condition of $M = 0.725$ and $\alpha = 3.5°$. The 3.5° angle of attack was chosen for altitude and weight to be equivalent to those of the design condition by approximately matching $M^2 C_L$. Data from the NTF test that encompass the two conditions are presented in figure 10 as a function of lift coefficient. The same data are replotted in figure 11 as a function of angle of attack for convenient comparison with TAWFIVE and WBPPW code results, which had a common angle of attack for the four configurations (figs. 12 to 14). The format of figure 10 is used, however, in the appendix where the WBPPW code comparisons are repeated on an individual lift-matched basis as explained subsequently.

TAWFIVE and WBPPW results, NTF data. Comparisons are presented between NTF data (ref. 3) and results from the TAWFIVE and WBPPW codes in figures 12 through 14. Each of these comparisons includes the baseline configuration and one of the three modified configurations. These comparisons, as well as the breakdown of the lift, pitching-moment, and drag coefficients by each code into wing and body contributions (not shown), provided the basis for the following observations.

The TAWFIVE code predicted lift coefficients with good accuracy, while those from the WBPPW code were consistently low. Both the wing and the body contributions to lift coefficient were lower for the WBPPW code than for the TAWFIVE code.

The nose-down pitching-moment coefficients were better predicted by the WBPPW code than by the TAWFIVE code. The TAWFIVE code nose-down pitching-moment coefficients were lower than those of the WBPPW code because the sign of the TAWFIVE body contribution was opposite (positive or nose-up) that of the WBPPW code. The way the body was modeled for each code and treated by each code affected the pitching-moment and drag coefficients. The body was modeled as axisymmetric for the TAWFIVE code and detailed for the WBPPW code. (Fig. 5 presents planform sketches.)

Drag coefficients were underpredicted by both codes. The drag coefficients from the TAWFIVE code were low partly because the body-friction drag contribution was not included in the calculations. The body-friction drag contribution from the WBPPW code (0.0062 for the cases in this report) accounts for a large part of the difference between the drag coefficients from the TAWFIVE code and the NTF data. The drag coefficients from the WBPPW code were low largely because the body was only modeled in the crude grid. This was observed after repeating two WBPPW cases using the fine body grid (one baseline case and the other with the combined modifications, both at $M = 0.800$ and $\alpha = 2.5°$). This observation could not have been made before the body-pressure drag was corrected as described in the section *WBPPW application.*

Incremental comparisons for the three modified configurations at both conditions are summarized in figure 15. There is overall agreement (between the NTF data and the predictions from the codes) that the trailing-edge modification had more effect on the transonic characteristics than did the leading-edge modification. Incremental lift and pitching-moment coefficients from both codes, as well as incremental drag coefficients from the TAWFIVE code, followed the trends of the NTF data. However, the drag-coefficient increments from the WBPPW code did not agree well with respect to the relative effects of the different modifications (the effect of the leading-edge modification was poorly predicted). As explained in the following paragraph, the WBPPW results were compared with NTF data in a different way in the appendix.

It is frequently desirable to match lift coefficients when making comparisons between computational results and experimental data. The preceding comparisons for a given Mach number are, of course, at a common angle of attack. The same computational results (at a given Mach number) can be compared with NTF data that are selected so that lift coefficients are matched on an individual basis for each configuration. Such a match was essentially made for each of the TAWFIVE results, since the predicted lift coefficients were within 6 percent of the NTF lift coefficients. The lift coefficients predicted by the WBPPW code, however, were as much as 20 percent low. Therefore, the preceding comparisons for the WBPPW code were repeated in the appendix with data whose lift coefficients were matched on an individual basis; the drag-coefficient increments agreed significantly better with these NTF data, but the trend of the drag-coefficient increment agreed with these NTF data only slightly better than with the data in figure 15.

Another comparison was made as a check on how the results might be affected by making predictions at a common lift coefficient. A final WBPPW comparison was made for the baseline and the combined modification at the design Mach number. It was made possible by computing an additional baseline case at $M = 0.800$ and $\alpha = 3.2°$ for which the lift coefficient (0.325) was approximately the same as the lift coefficient of 0.323 for the configuration with the combined modifications. Results for these two configurations are given in figure 16 (format of fig. 10(b)), and corresponding incremental results are given in figure 17.

The pitching-moment coefficients were again in good agreement, and the drag coefficients were still underpredicted (fig. 16). For this comparison, the predicted angle-of-attack increment (rather than ΔC_L) was shown and differed by only 0.12° from the NTF increment (fig. 17). The computed increment in pitching-moment coefficient in this case (fig. 17) differed from the NTF data by the same amount (0.010) as it did at a common angle of attack (fig. 15(b)). The WBPPW drag-coefficient increment for the combined modification was negative; nevertheless, the increment was lower than that from the NTF data by a smaller amount (−0.0027) in figure 17 than the amount (−0.0038) in figure 15(b).

Concluding Remarks

Computational predictions of the effects of wing contour modifications on maximum lift and transonic performance were made and verified against low-speed and transonic wind-tunnel data for an electronics countermeasures aircraft. The predictions were based on results from three computer codes that include viscous effects. Maximum lift coefficients were predicted with MCARF, a two-dimensional subsonic panel code. Transonic performance was predicted with TAWFIVE, a full-potential method, and WBPPW, a small-disturbance potential-flow method. The modifications were previously designed with the aid of these and other codes. The wing modifications consisted of contour

changes to the leading-edge slats and trailing-edge flaps. The leading-edge slats were made more blunt and slightly drooped in the outboard regions. The trailing-edge flaps were made more cambered and slightly thickened at the base. The modifications were designed for increased maximum lift with minimum effect on transonic performance.

The effects of the modifications on low-speed maximum lift coefficient were predicted two dimensionally and three dimensionally at two Reynolds numbers. The predictions from the two-dimensional (2D) low-speed code exhibited the same trends as the corresponding 2D experimental data. The code also predicted whether transition occurred before, at, or after a transition strip location and which phenomenon was responsible for stall, but these results were not verified experimentally. Three-dimensional (3D) estimates, based on results from the 2D code, overpredicted the effect of the leading-edge modification but agreed well with 3D experimental data for the effect of the trailing-edge modification. The experimental data were influenced by Reynolds number effects that were not predicted by the estimates. Nevertheless, at the higher of the two Reynolds numbers, the estimates and the experimental data showed a significant increase in the maximum-lift-coefficient increment for the combined leading- and trailing-edge modification over that for the trailing-edge modification alone.

Effects of the modifications on transonic lift, pitching-moment, and drag coefficients were predicted by both the TAWFIVE and WBPPW codes. During the application of the TAWFIVE code, some minor problems related to the computation of the wing-body grid and the wing boundary layer had to be resolved. Results from both codes were compared with experimental data for a common angle of attack. Since the WBPPW code consistently underpredicted the lift coefficient for a given angle of attack, results from that code were also compared with lift-matched experimental data. The question of whether to match lift coefficient was not important for the TAWFIVE code because it predicted lift coefficient accurately. Future drag predictions could be improved by including the body-friction effect in the TAWFIVE code and by using the fine body grid after correcting the body-drag calculation in the WBPPW code.

There was overall agreement between the experimental data and code results, in that the trailing-edge and combined modifications had more effect on the transonic characteristics than did the leading-edge modification. The relative effects of the modifications on transonic lift and pitching-moment coefficients were well predicted by both codes. The relative effects of the modifications on transonic drag coefficient were well predicted by the TAWFIVE code but poorly predicted by the WBPPW code.

NASA Langley Research Center
Hampton, VA 23665-5225
August 27, 1990

Appendix

WBPPW Results, NTF Data

A comparison was made in which the lift coefficients were matched between NTF (National Transonic Facility) data and results from the WBPPW code (a transonic, small-disturbance, potential-flow code). The WBPPW results are from figures 12 to 15. The NTF data were interpolated so that at a given Mach number the lift coefficient matched the computed lift coefficient for each individual configuration. This, of course, meant that even when the WBPPW code results for all four configurations were at one angle of attack, these NTF data were at different angles from each other.

The comparisons were plotted in figures 18 to 20 in the format of figure 10, as a function of lift coefficient. Incremental comparisons were summarized in figure 21, where $\Delta\alpha$ was included rather than ΔC_L. The incremental angle of attack agreed to within about one-third of a degree between the WBPPW results and these NTF data. The trend of the pitching-moment-coefficient increment was in good agreement with these data for both conditions, as it was with the data in figure 15. For both conditions, the trend of the drag-coefficient increment agreed slightly better with these NTF data than with the data in figure 15.

The drag-coefficient increments agreed significantly better with these NTF data than with the data in figure 15. In particular, the predicted increment for the combined modification at $M = 0.800$ was 0.0016 below the increment from these NTF data (fig. 21(b)) but 0.0038 below that from the data in figure 15(b).

References

1. Hanley, Robert J.: Development of an Airframe Modification To Improve the Mission Effectiveness of the EA-6B Airplane. *A Collection of Technical Papers AIAA 5th Applied Aerodynamics Conference,* Aug. 1987, pp. 241–247. (Available as AIAA-87-2358.)
2. Sewall, W. G.; McGhee, R. J.; and Ferris, J. C.: Wind-Tunnel Test Results of Airfoil Modifications for the EA-6B. *A Collection of Technical Papers AIAA 5th Applied Aerodynamics Conference,* Aug. 1987, pp. 248–256. (Available as AIAA-87-2359.)
3. Waggoner, E. G.; and Allison, D. O.: EA-6B High-Lift Wing Modifications: *A Collection of Technical Papers AIAA 5th Applied Aerodynamics Conference,* Aug. 1987, pp. 257–269. (Available as AIAA-87-2360.)
4. Jordan, Frank L., Jr.; Hahne, David E.; Masiello, Matthew F.; and Gato, William: High Angle-of-Attack Stability and Control Improvements for the EA-6B Prowler. *A Collection of Technical Papers AIAA 5th Applied Aerodynamics Conference,* Aug. 1987, pp. 270–285. (Available as AIAA-87-2361.)
5. Gato, W.; and Masiello, M. F.: Innovative Aerodynamics: The Sensible Way of Restoring Growth Capability to the EA-6B Prowler. *A Collection of Technical Papers—AIAA 5th Applied Aerodynamics Conference,* Aug. 1987, pp. 286–299. (Available as AIAA-87-2362.)
6. Stevens, W. A.; Goradia, S. H.; and Braden, J. A.: *Mathematical Model for Two-Dimensional Multi-Component Airfoils in Viscous Flow.* NASA CR-1843, 1971.
7. Brune, G. W.; and Manke, J. W.: *An Improved Version of the NASA-Lockheed Multielement Airfoil Analysis Computer Program.* NASA CR-145323, 1978.
8. Cohen, Clarence B.; and Reshotko, Eli: *The Compressible Laminar Boundary Layer With Heat Transfer and Arbitrary Pressure Gradient.* NACA Rep. 1294, 1956. (Supersedes NACA TN 3326.)
9. Schlichting, H.; and Ulrich, A.: Zur Berechnung des Umschlages Laminar/Turbulent. *Jahrb. 1942 der deutschen Luftfahrtforschung,* R. Oldenbourg (Munich), pp. I 8–I 35.
10. Granville, Paul S.: *The Calculation of the Viscous Drag of Bodies of Revolution.* Rep. 849, David W. Taylor Model Basin, July 1953.
11. Morgan, Harry L.: High-Lift Flaps for Natural Laminar Flow Airfoils. *Laminar Flow Aircraft Certification,* Louis J. Williams, compiler, NASA CP-2413, 1986, pp. 31–65.
12. Melson, N. Duane; and Streett, Craig L.: *TAWFIVE: A Users' Guide.* NASA TM-84619, 1983.
13. Caughey, D. A.; and Jameson, Antony: Recent Progress in Finite-Volume Calculations for Wing-Fuselage Combinations. AIAA Paper 79-1513, July 1979.
14. Stock, H. W.: *Integral Method for the Calculation of Three-Dimensional, Laminar and Turbulent Boundary Layers.* NASA TM-75320, 1978.
15. Smith, P. D.: *An Integral Prediction Method for Three-Dimensional Compressible Turbulent Boundary Layers.* R. & M. No. 3739, British Aeronautical Research Council, 1974.
16. Streett, Craig L.: *Viscous-Inviscid Interaction Method Including Wake Effects for Three-Dimensional Wing-Body Configurations.* NASA TP-1910, 1981.
17. Streett, Craig L.: Viscous-Inviscid Interaction for Transonic Wing-Body Configurations Including Wake Effects. *AIAA J.,* vol. 20, no. 7, July 1982, pp. 915–923.
18. Boppe, Charles W.: *Aerodynamic Analysis for Aircraft With Nacelles, Pylons, and Winglets at Transonic Speeds.* NASA CR-4066, 1987.
19. Waggoner, Edgar G.: Validation of a Transonic Analysis Code for Use in Preliminary Design of Advanced Transport Configurations. *ICAS Proceedings, 1984 14th Congress of the International Council of the Aeronautical Sciences,* Volume 1, B. Laschka and R. Staufenbiel, eds., Sept. 1984, pp. 377–390. (Available as ICAS-84-1.4.2.)
20. Bradshaw, P.; and Ferriss, D. H.: Calculation of Boundary-Layer Development Using the Turbulent Energy Equation: Compressible Flow on Adiabatic Walls. *J. Fluid Mech.,* vol. 46, pt. 1, Mar. 15, 1971, pp. 83–110.
21. Mason, William H.; Mackenzie, Donald; Stern, Mark; Ballhaus, William F.; and Frick, Juanita: *An Automated Procedure for Computing the Three-Dimensional Transonic Flow Over Wing-Body Combinations, Including Viscous Effects. Volume I—Description of Analysis Methods and Applications.* AFFDL-TR-77-122, Vol. I, Feb. 1978. (Available from DTIC as AD A055 899.)
22. Boppe, Charles W.: *Transonic Flow Field Analysis for Wing-Fuselage Configurations.* NASA CR-3243, 1980.

Table I. Streamwise Airfoil Coordinates for Inboard Design Station

$[\eta = 0.28;\ t/c = 0.087]$

	bl		*le* and *Te*		*le* and *te*	
x/c	$(y/c)_u$	$(y/c)_l$	$(y/c)_u$	$(y/c)_l$	$(y/c)_u$	$(y/c)_l$
0.00000	0.00041	0.00041	0.00049	0.00049	0.00049	0.00049
.00100	.00380	−.00240	.00497	−.00378	.00497	−.00378
.00300	.00661	−.00433	.00828	−.00657	.00828	−.00657
.00500	.00847	−.00562	.01053	−.00821	.01053	−.00821
.00700	.00995	−.00659	.01229	−.00931	.01229	−.00931
.01000	.01184	−.00774	.01441	−.01046	.01441	−.01046
.02000	.01673	−.01010	.01952	−.01251	.01952	−.01251
.03000	.02065	−.01160	.02335	−.01362	.02335	−.01362
.04000	.02403	−.01281	.02652	−.01442	.02652	−.01442
.05000	.02702	−.01384	.02924	−.01508	.02924	−.01508
.06000	.02973	−.01473	.03162	−.01565	.03162	−.01565
.08000	.03443	−.01627	.03569	−.01672	.03569	−.01672
.10000	.03839	−.01763	.03912	−.01782	.03912	−.01782
.12000	.04179	−.01890	.04212	−.01896	.04212	−.01896
.14000	.04471	−.02011	.04480	−.02013	.04480	−.02013
.16000	.04721	−.02129	.04721	−.02129	.04721	−.02129
.18000	.04933	−.02243	.04933	−.02243	.04933	−.02243
.20000	.05119	−.02353	.05119	−.02353	.05119	−.02353
.25000	.05451	−.02613	.05451	−.02613	.05451	−.02613
.30000	.05633	−.02834	.05633	−.02834	.05633	−.02834
.35000	.05688	−.02999	.05688	−.02999	.05688	−.02999
.40000	.05623	−.03088	.05623	−.03088	.05623	−.03088
.45000	.05453	−.03091	.05453	−.03091	.05453	−.03091
.50000	.05186	−.03014	.05186	−.03014	.05186	−.03014
.55000	.04830	−.02866	.04830	−.02866	.04830	−.02866
.60000	.04406	−.02661	.04406	−.02661	.04406	−.02661
.65000	.03926	−.02397	.03926	−.02397	.03926	−.02397
.70000	.03400	−.02090	.03400	−.02088	.03400	−.02088
.75000	.02843	−.01749	.02843	−.01695	.02843	−.01695
.80000	.02283	−.01408	.02283	−.01162	.02283	−.01162
.82000	.02059	−.01271	.02063	−.00900	.02063	−.00900
.84000	.01835	−.01135	.01846	−.00614	.01846	−.00614
.86000	.01611	−.00998	.01635	−.00324	.01635	−.00324
.88000	.01387	−.00862	.01441	−.00062	.01440	−.00062
.90000	.01163	−.00725	.01268	.00151	.01248	.00151
.92000	.00939	−.00588	.01111	.00298	.01054	.00298
.94000	.00715	−.00452	.00968	.00358	.00859	.00358
.95000	.00603	−.00384	.00903	.00345	.00762	.00345
.96000	.00490	−.00315	.00846	.00296	.00665	.00296
.97000	.00378	−.00247	.00798	.00209	.00568	.00209
.98000	.00266	−.00179	.00762	.00078	.00471	.00078
.99000	.00154	−.00111	.00740	−.00103	.00374	−.00103
1.00000	.00042	−.00042	.00735	−.00338	.00277	−.00338

Table II. Streamwise Airfoil Coordinates for Outboard Design Station

$[\eta = 0.75;\ t/c = 0.074]$

	bl		*le* and *Te*		*le* and *te*	
x/c	$(y/c)_u$	$(y/c)_l$	$(y/c)_u$	$(y/c)_l$	$(y/c)_u$	$(y/c)_l$
0.00000	−0.00263	−0.00263	−0.00600	−0.00600	−0.00600	−0.00600
.00100	.00101	−.00464	−.00193	−.00959	−.00193	−.00959
.00300	.00320	−.00621	.00114	−.01168	.00114	−.01168
.00500	.00483	−.00720	.00323	−.01283	.00323	−.01283
.00700	.00613	−.00796	.00488	−.01356	.00488	−.01356
.01000	.00785	−.00882	.00695	−.01427	.00695	−.01427
.02000	.01252	−.01052	.01218	−.01526	.01218	−.01526
.03000	.01627	−.01135	.01621	−.01545	.01621	−.01545
.04000	.01948	−.01199	.01959	−.01539	.01959	−.01539
.05000	.02227	−.01251	.02252	−.01522	.02252	−.01522
.06000	.02481	−.01295	.02512	−.01504	.02512	−.01504
.08000	.02933	−.01363	.02959	−.01483	.02959	−.01483
.10000	.03315	−.01430	.03334	−.01490	.03334	−.01490
.12000	.03645	−.01499	.03654	−.01522	.03654	−.01522
.14000	.03925	−.01568	.03928	−.01574	.03928	−.01574
.16000	.04161	−.01640	.04162	−.01640	.04162	−.01640
.18000	.04360	−.01712	.04360	−.01712	.04360	−.01712
.20000	.04527	−.01787	.04527	−.01787	.04527	−.01787
.25000	.04834	−.01979	.04834	−.01979	.04834	−.01979
.30000	.05005	−.02158	.05005	−.02158	.05005	−.02158
.35000	.05053	−.02303	.05053	−.02303	.05053	−.02303
.40000	.04992	−.02403	.04992	−.02403	.04992	−.02403
.45000	.04834	−.02436	.04834	−.02436	.04834	−.02436
.50000	.04588	−.02380	.04588	−.02380	.04588	−.02380
.55000	.04265	−.02268	.04265	−.02268	.04265	−.02268
.60000	.03882	−.02118	.03882	−.02118	.03882	−.02118
.65000	.03455	−.01924	.03455	−.01924	.03455	−.01924
.70000	.02999	−.01686	.02999	−.01689	.02999	−.01689
.75000	.02529	−.01432	.02529	−.01384	.02529	−.01384
.80000	.02051	−.01172	.02051	−.00961	.02051	−.00961
.82000	.01858	−.01066	.01861	−.00750	.01861	−.00750
.84000	.01663	−.00960	.01673	−.00516	.01673	−.00516
.86000	.01469	−.00853	.01490	−.00279	.01490	−.00279
.88000	.01274	−.00746	.01320	−.00065	.01319	−.00065
.90000	.01079	−.00639	.01168	.00107	.01151	.00107
.92000	.00884	−.00532	.01030	.00223	.00982	.00223
.94000	.00689	−.00425	.00904	.00265	.00812	.00265
.95000	.00591	−.00372	.00847	.00249	.00728	.00249
.96000	.00494	−.00318	.00797	.00203	.00643	.00203
.97000	.00397	−.00265	.00754	.00124	.00558	.00124
.98000	.00300	−.00212	.00722	.00007	.00474	.00007
.99000	.00203	−.00159	.00702	−.00152	.00389	−.00152
1.00000	.00107	−.00107	.00698	−.00359	.00304	−.00359

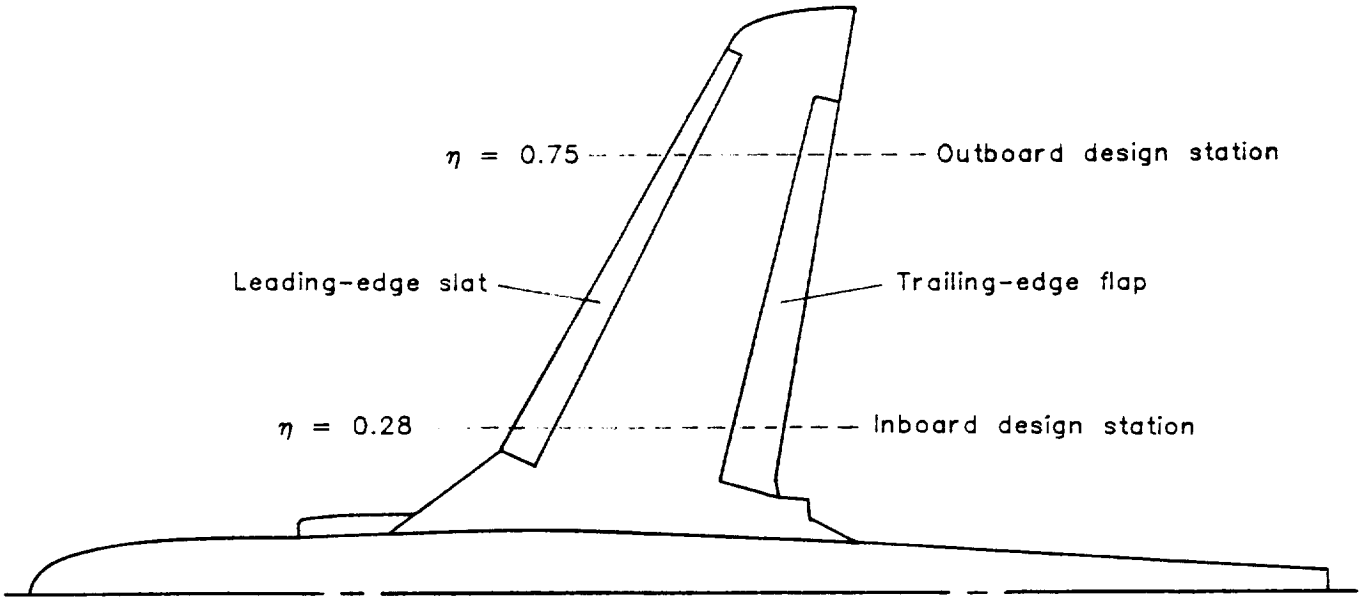

Figure 1. Planform sketch of wing-body configuration.

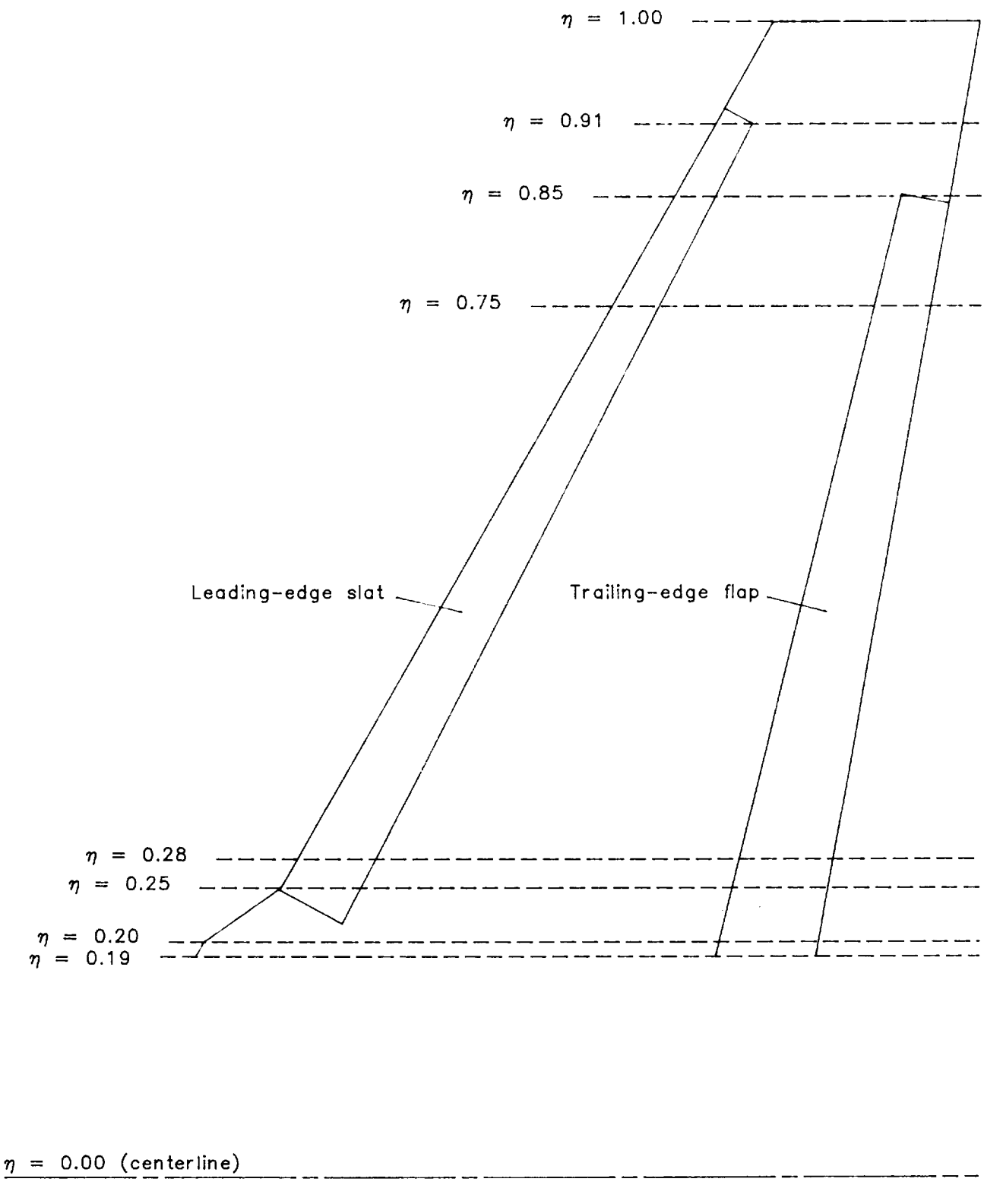

Figure 2. Planform sketch of wing showing spanwise positions of slats and flaps.

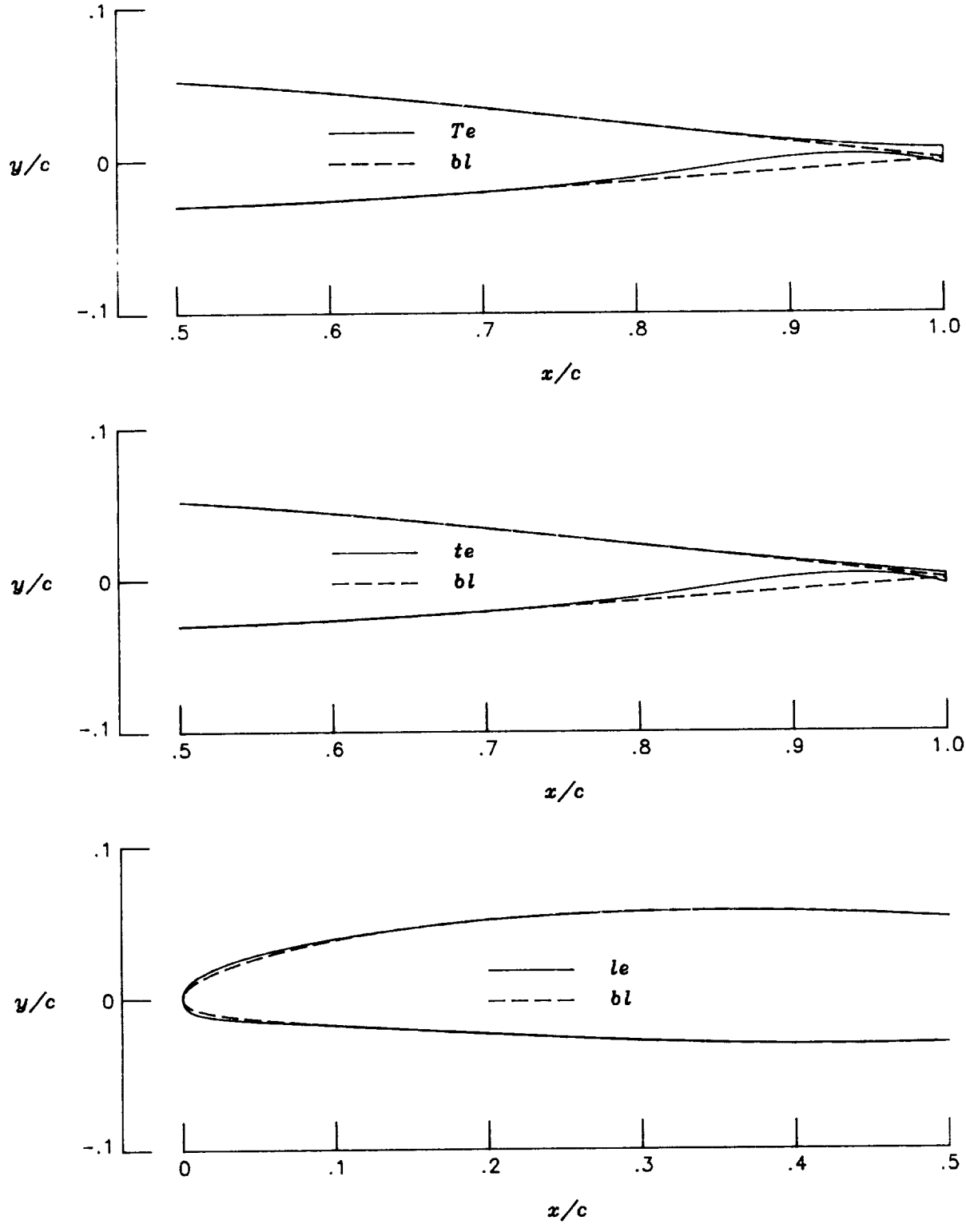

Figure 3. Airfoil modifications for inboard design station. $\eta = 0.28$; $t/c = 0.087$.

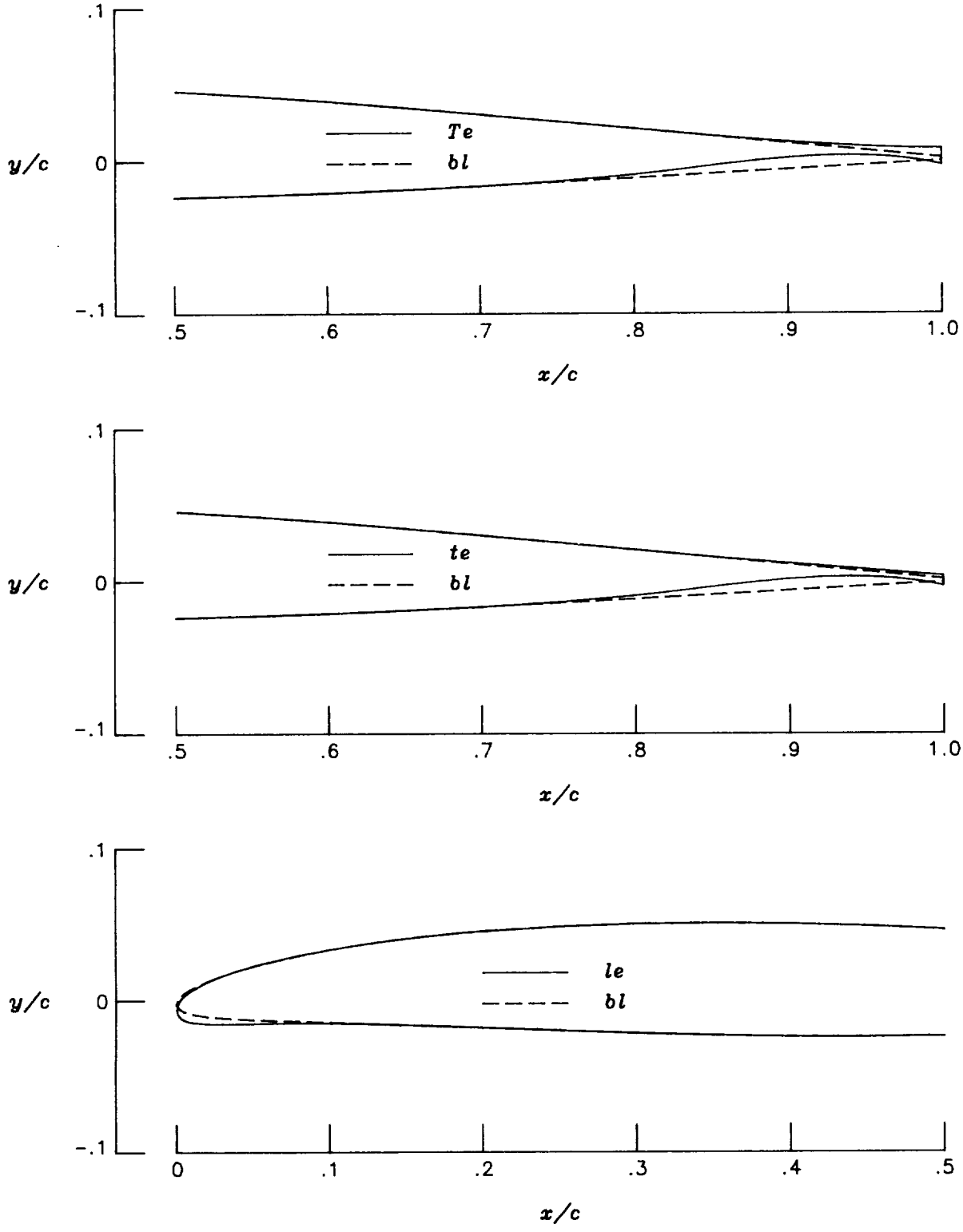

Figure 4. Airfoil modifications for outboard design station. $\eta = 0.75$; $t/c = 0.074$.

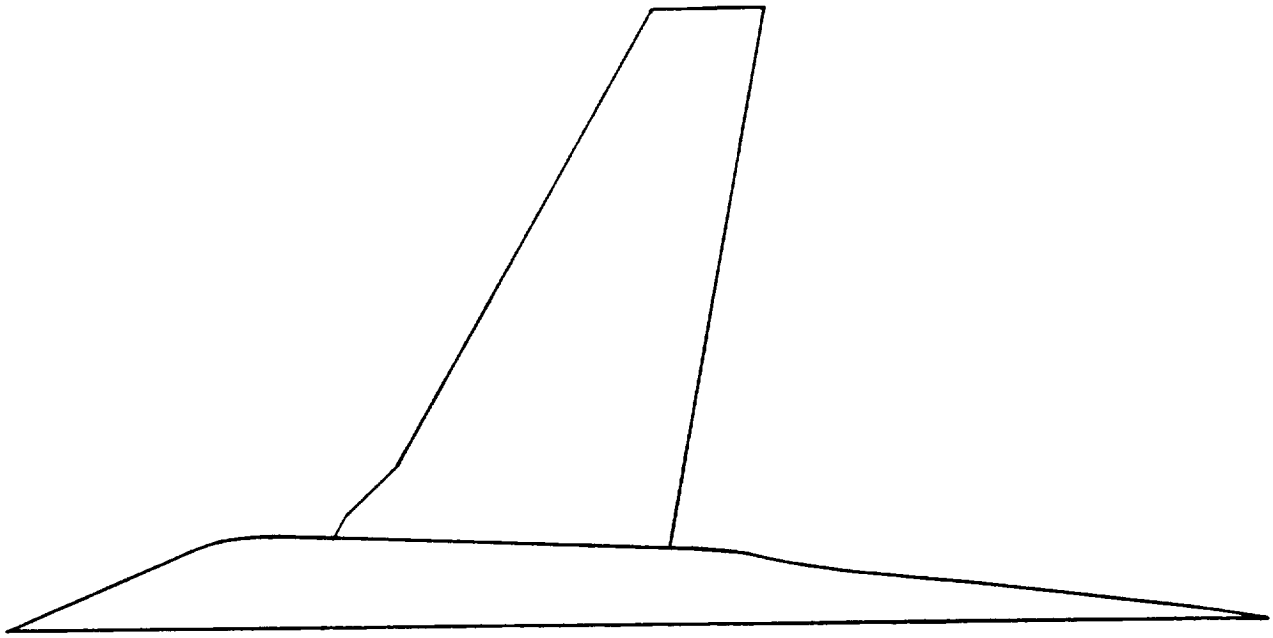

(a) TAWFIVE code.

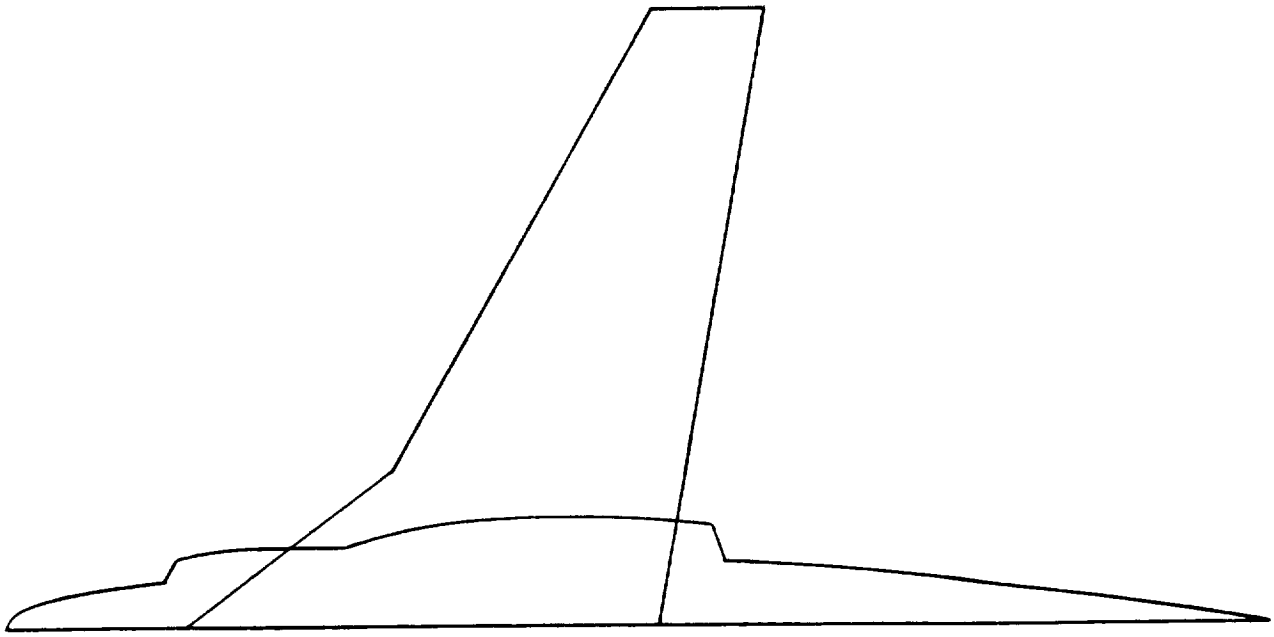

(b) WBPPW code.

Figure 5. Planform sketches of wing-body as modeled in application of each transonic code.

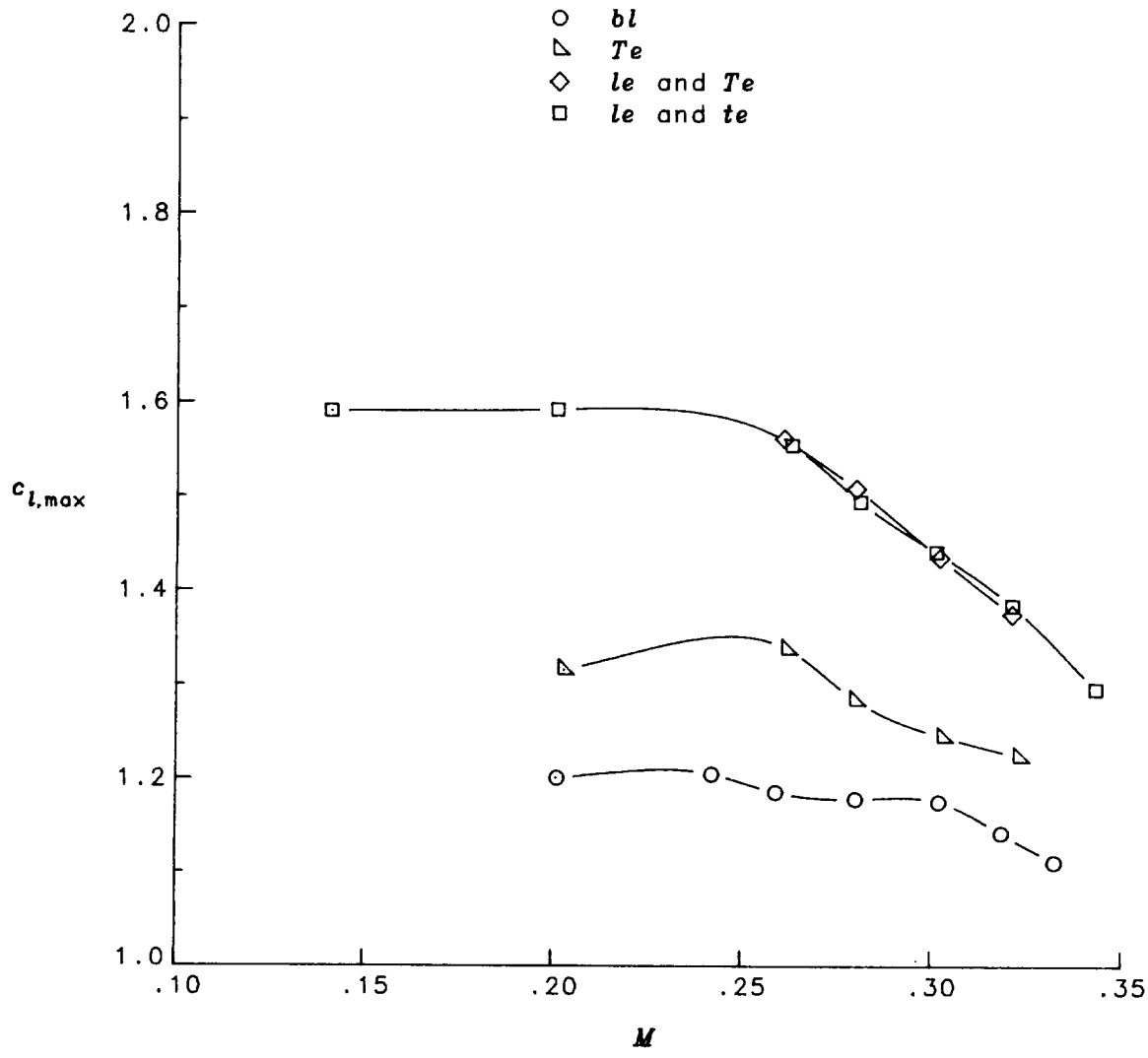

Figure 6. Maximum-lift-coefficient data from LTPT test (ref. 2) for inboard-station airfoils. $R = 10 \times 10^6$.

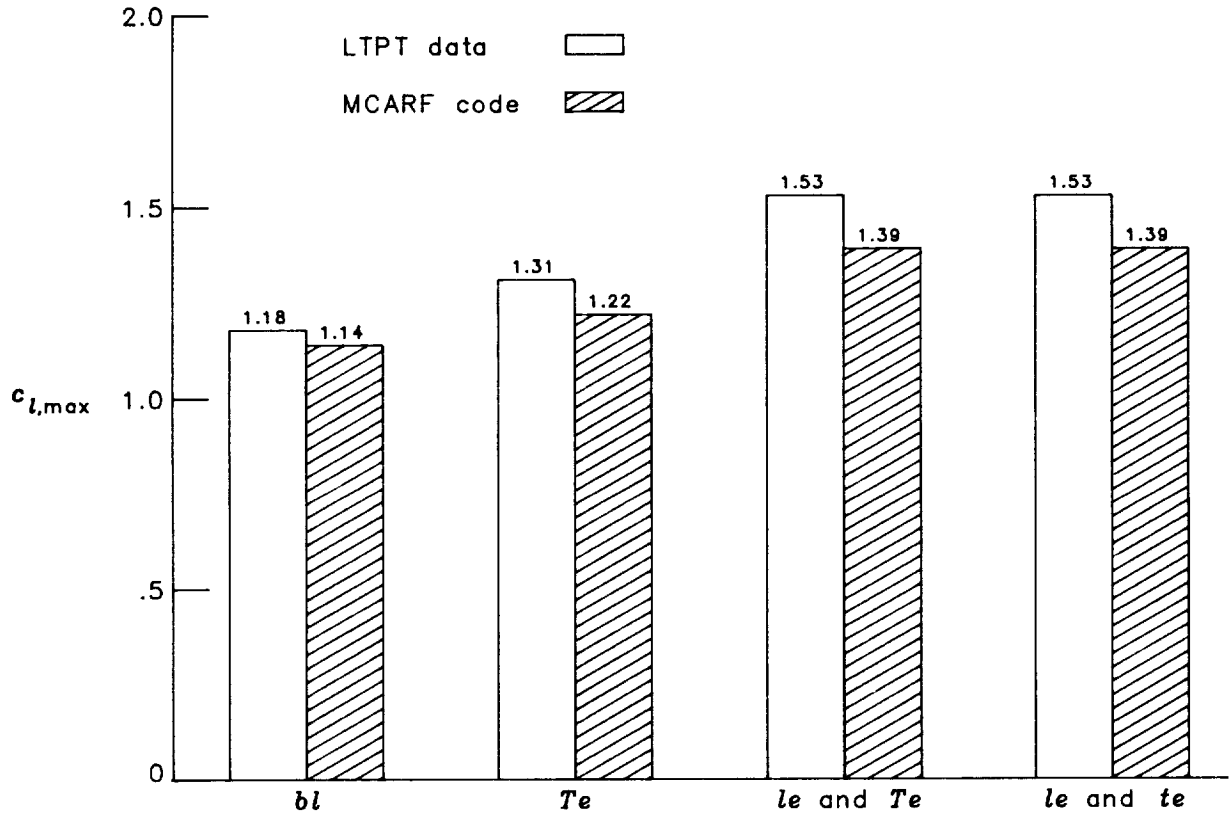

(a) Maximum lift coefficient.

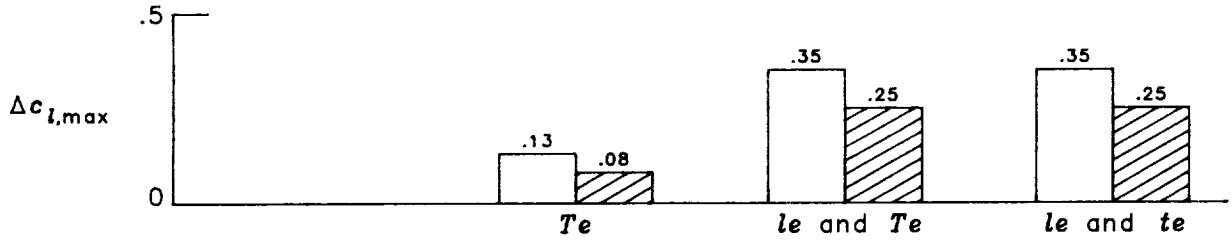

(b) Incremental maximum lift coefficient.

Figure 7. Comparison of MCARF results with LTPT data for inboard-station airfoils. $M = 0.271$; $R = 10 \times 10^6$.

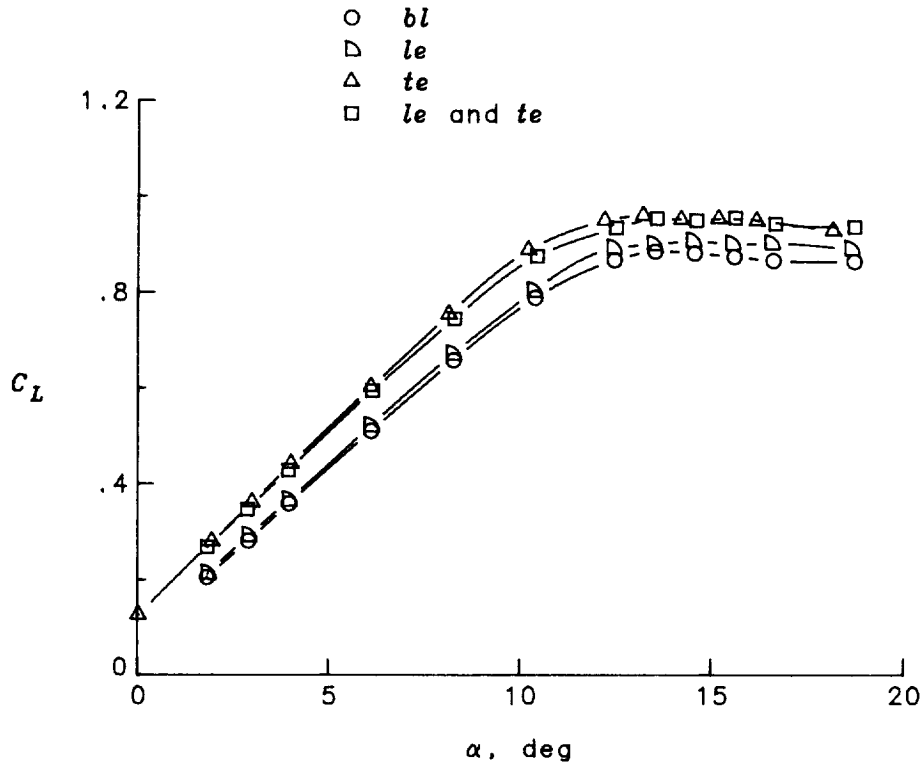

(a) $R = 1.4 \times 10^6$.

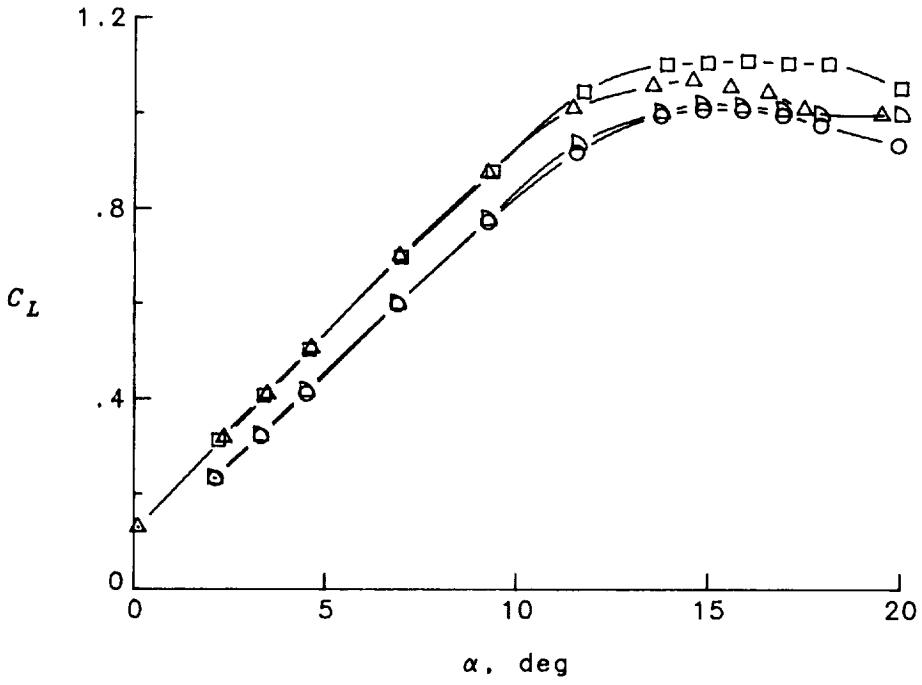

(b) $R = 5.4 \times 10^6$.

Figure 8. Lift-coefficient data from NTF test (ref. 3). $M = 0.3$.

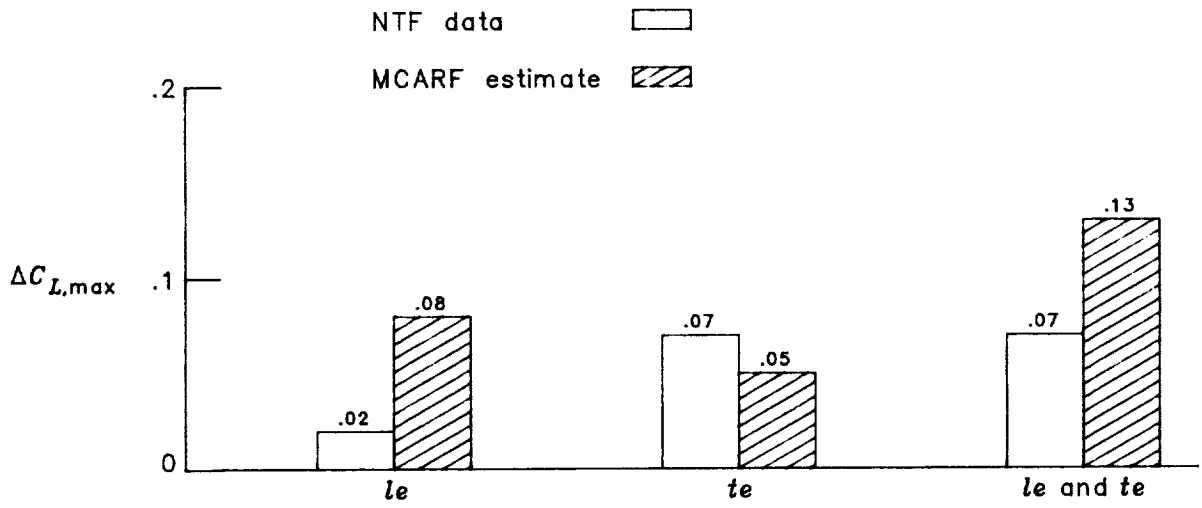

(a) $R = 1.4 \times 10^6$.

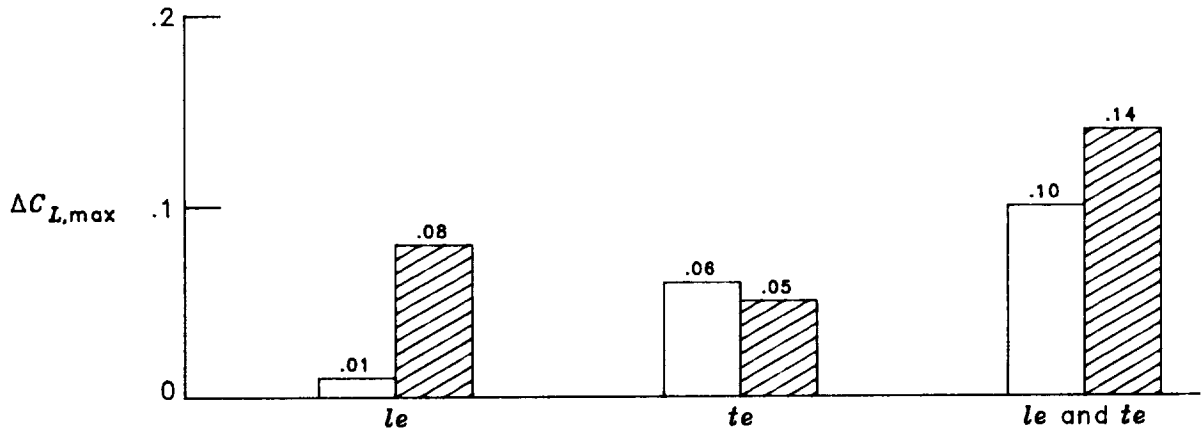

(b) $R = 5.4 \times 10^6$.

Figure 9. Comparison of results for estimated incremental maximum lift coefficient with NTF data. $M = 0.3$.

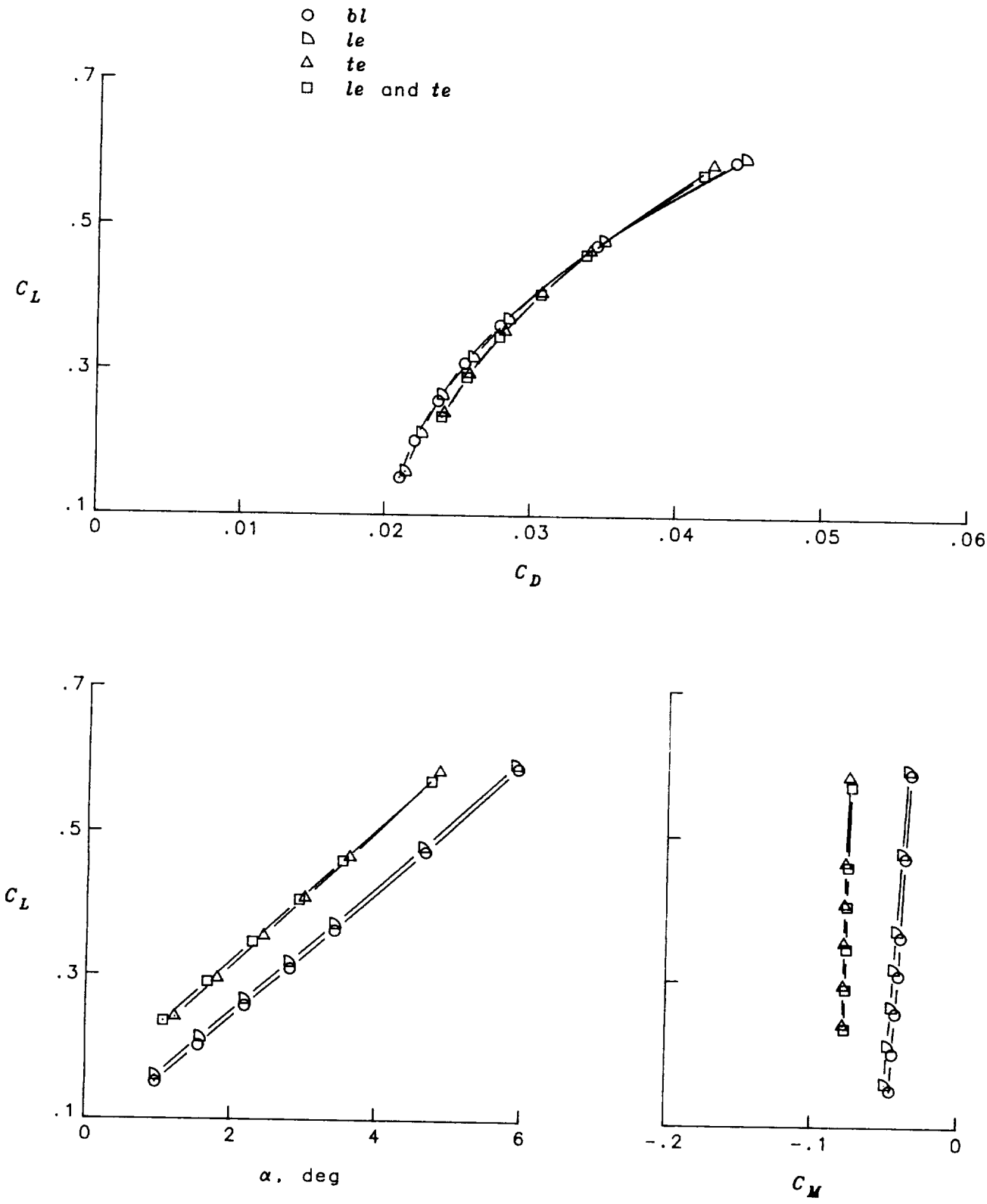

(a) $M = 0.725$.

Figure 10. Aerodynamic data from NTF test (ref. 3) as a function of C_L. $R = 2.7 \times 10^6$.

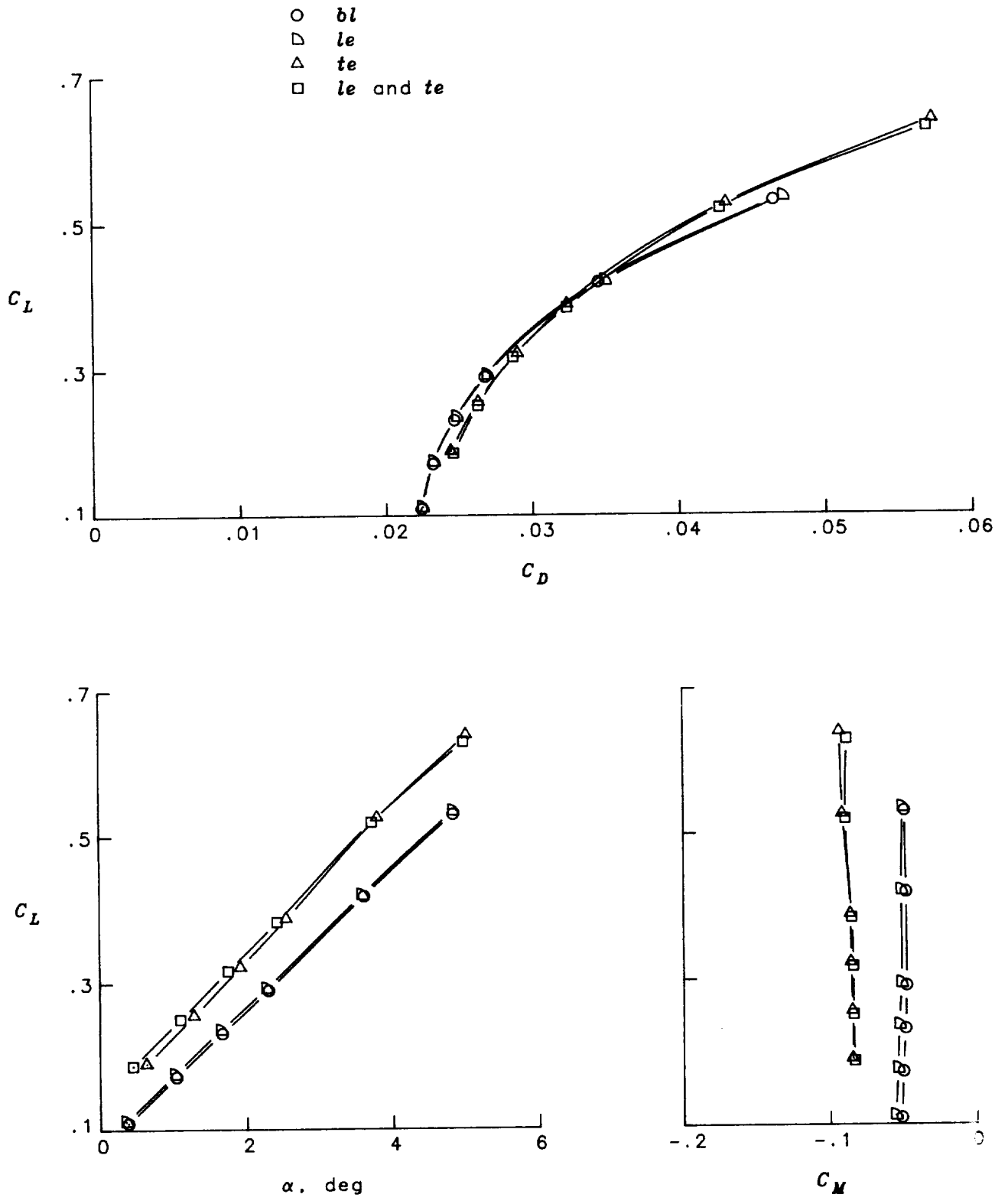

(b) $M = 0.800$.

Figure 10. Concluded.

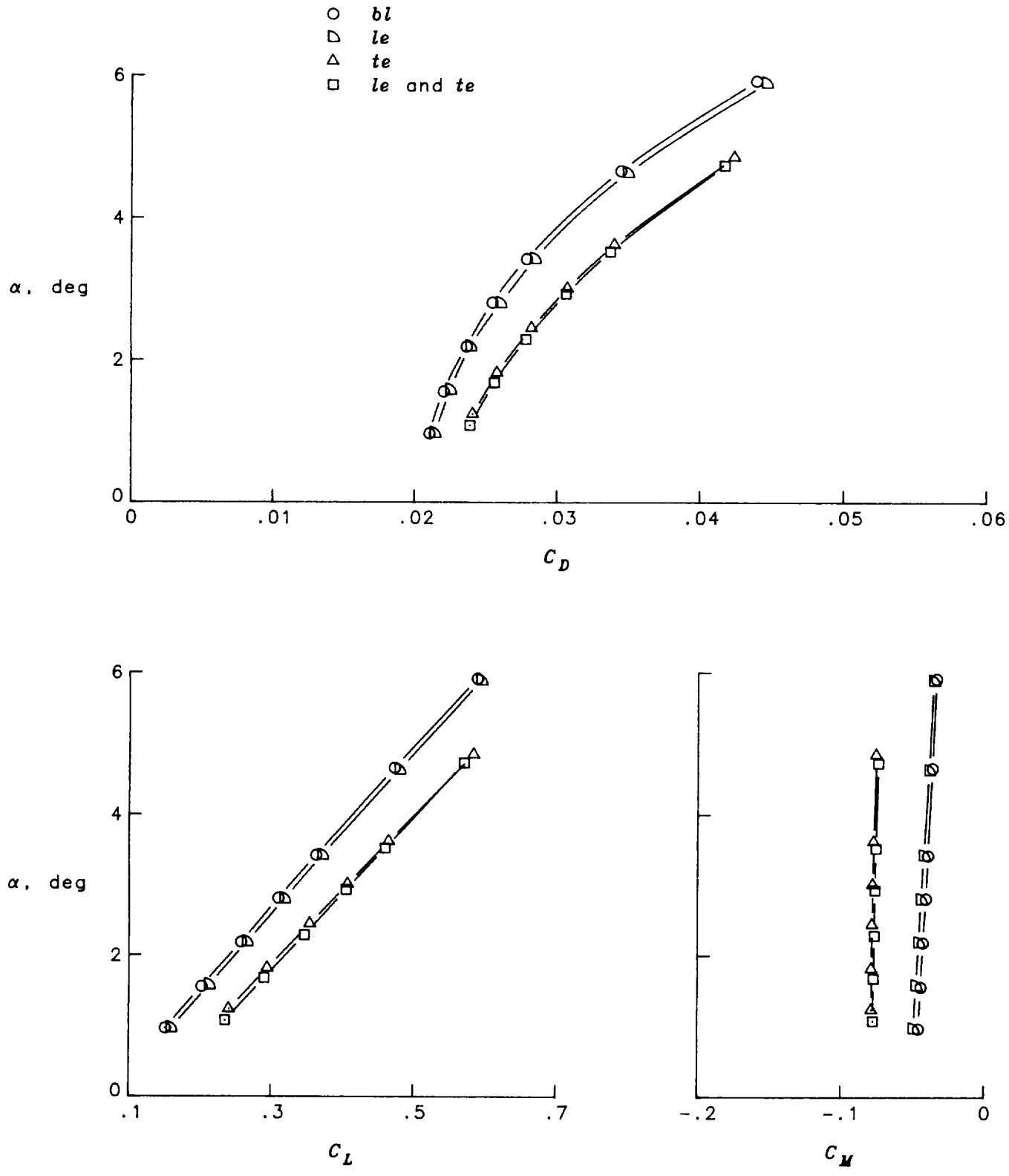

(a) $M = 0.725$.

Figure 11. Aerodynamic data from NTF test (ref. 3) as a function of α. $R = 2.7 \times 10^6$.

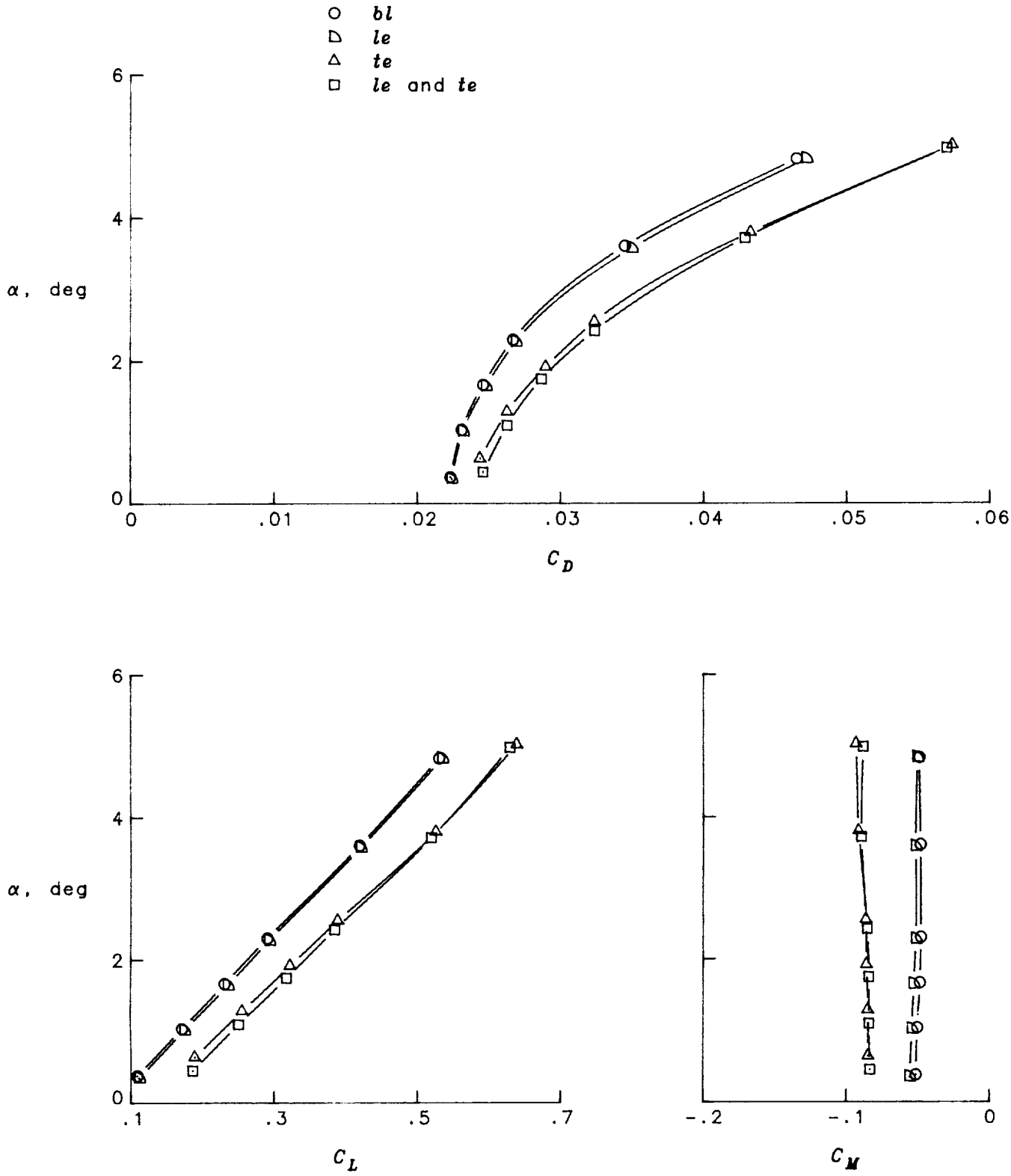

(b) $M = 0.800$.

Figure 11. Concluded.

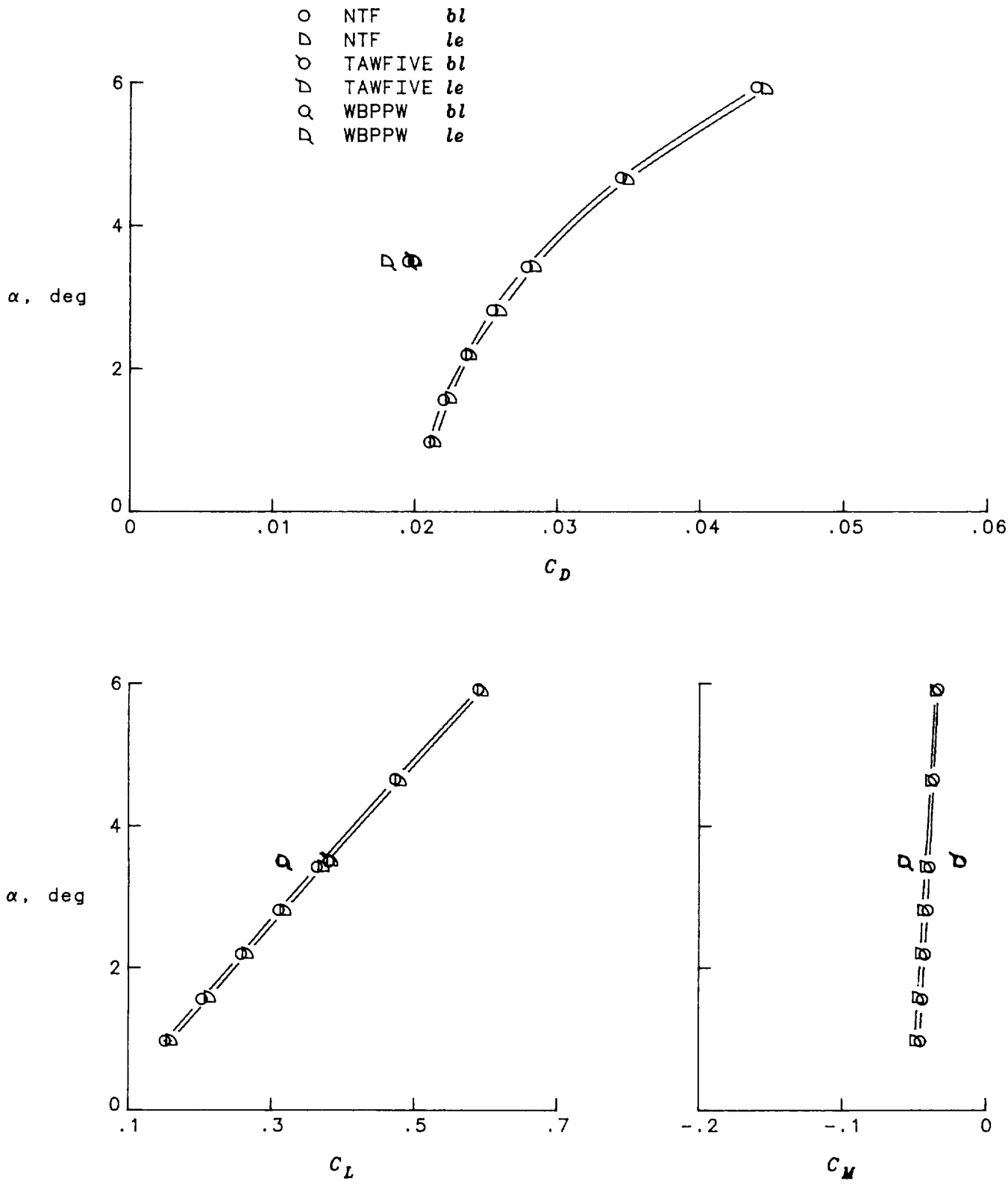

(a) $M = 0.725$.

Figure 12. Comparison of predicted effects of leading-edge modification with NTF data. $R = 2.7 \times 10^6$.

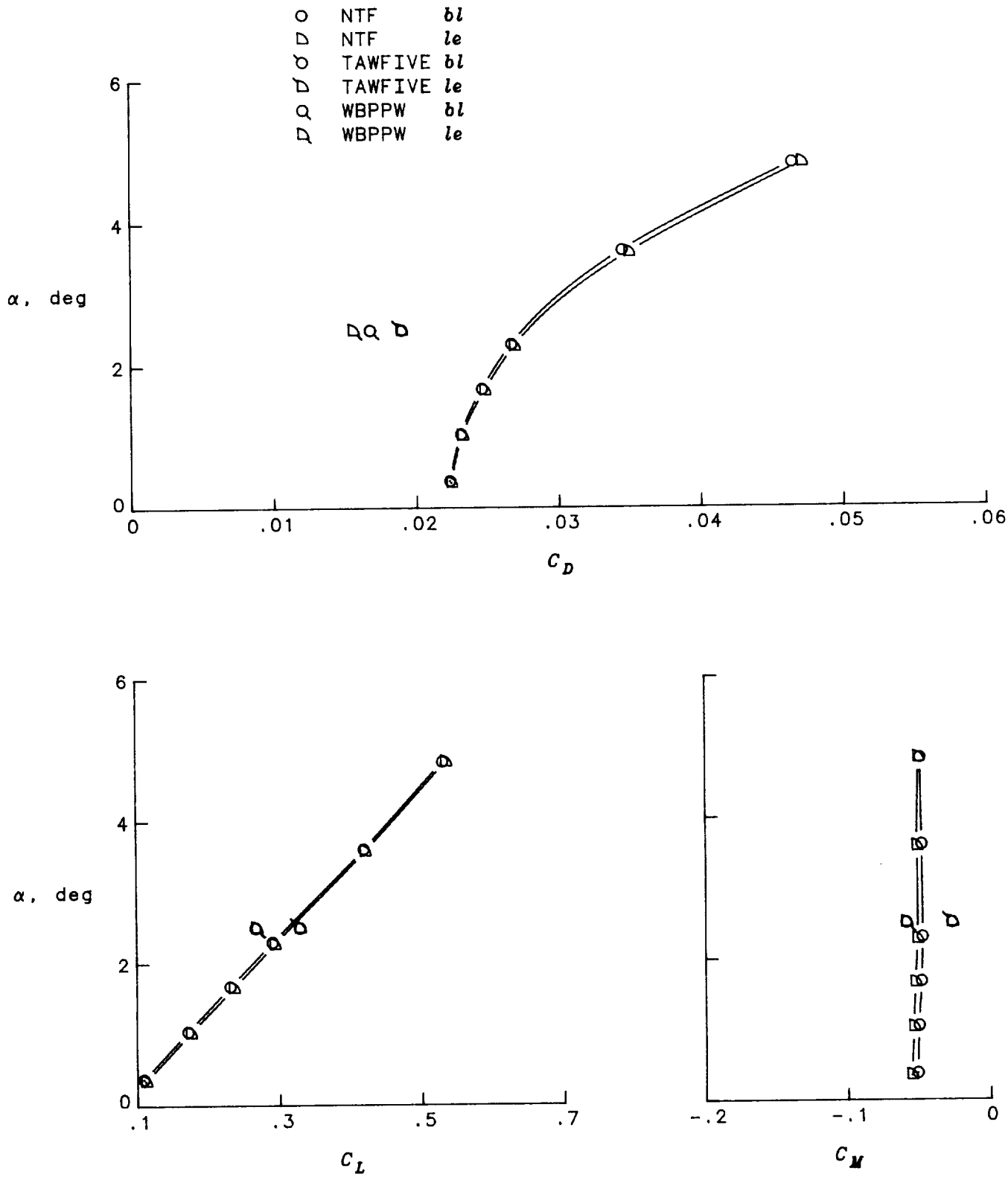

(b) $M = 0.800$.

Figure 12. Concluded.

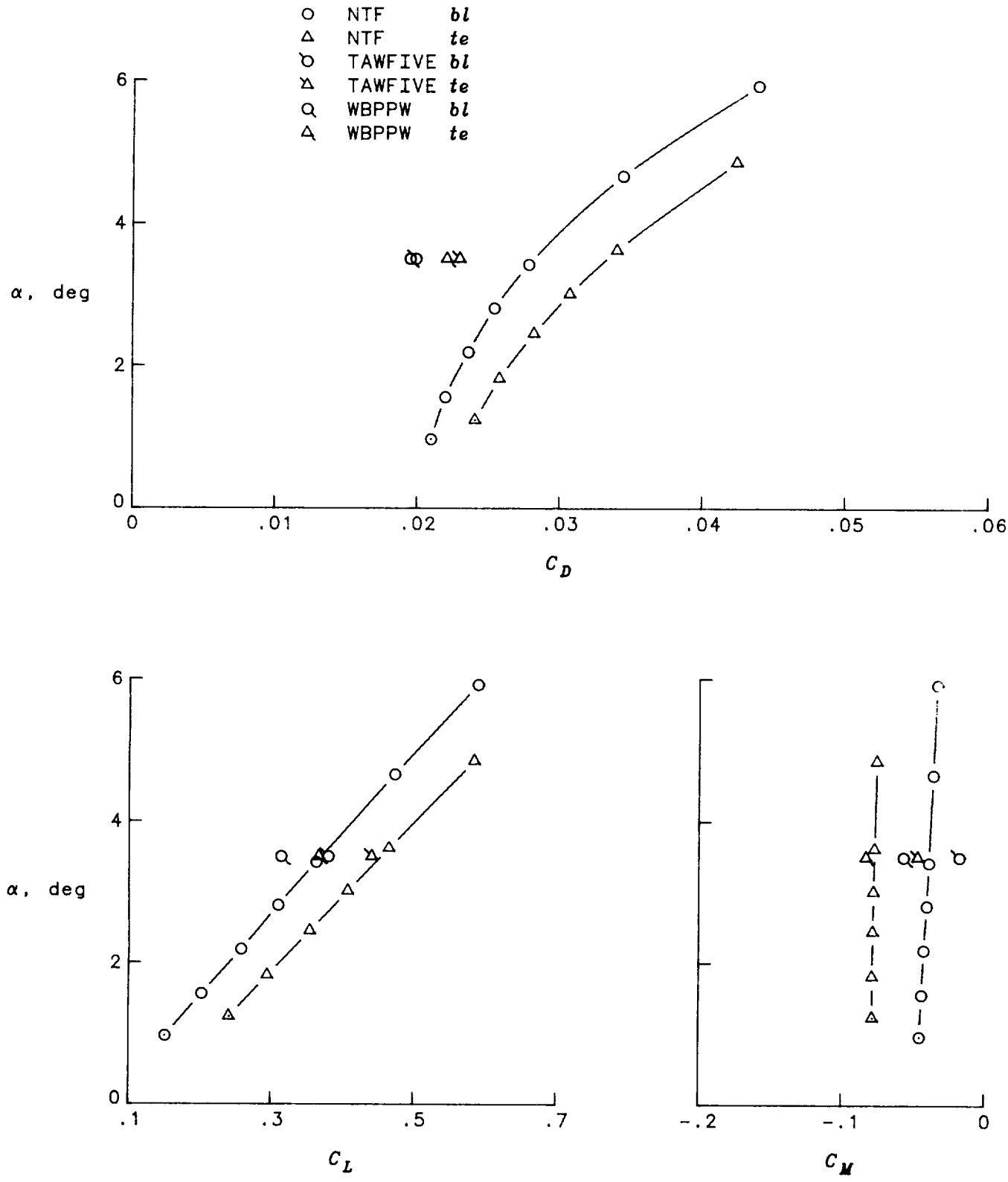

(a) $M = 0.725$.

Figure 13. Comparison of predicted effects of trailing-edge modification with NTF data. $R = 2.7 \times 10^6$.

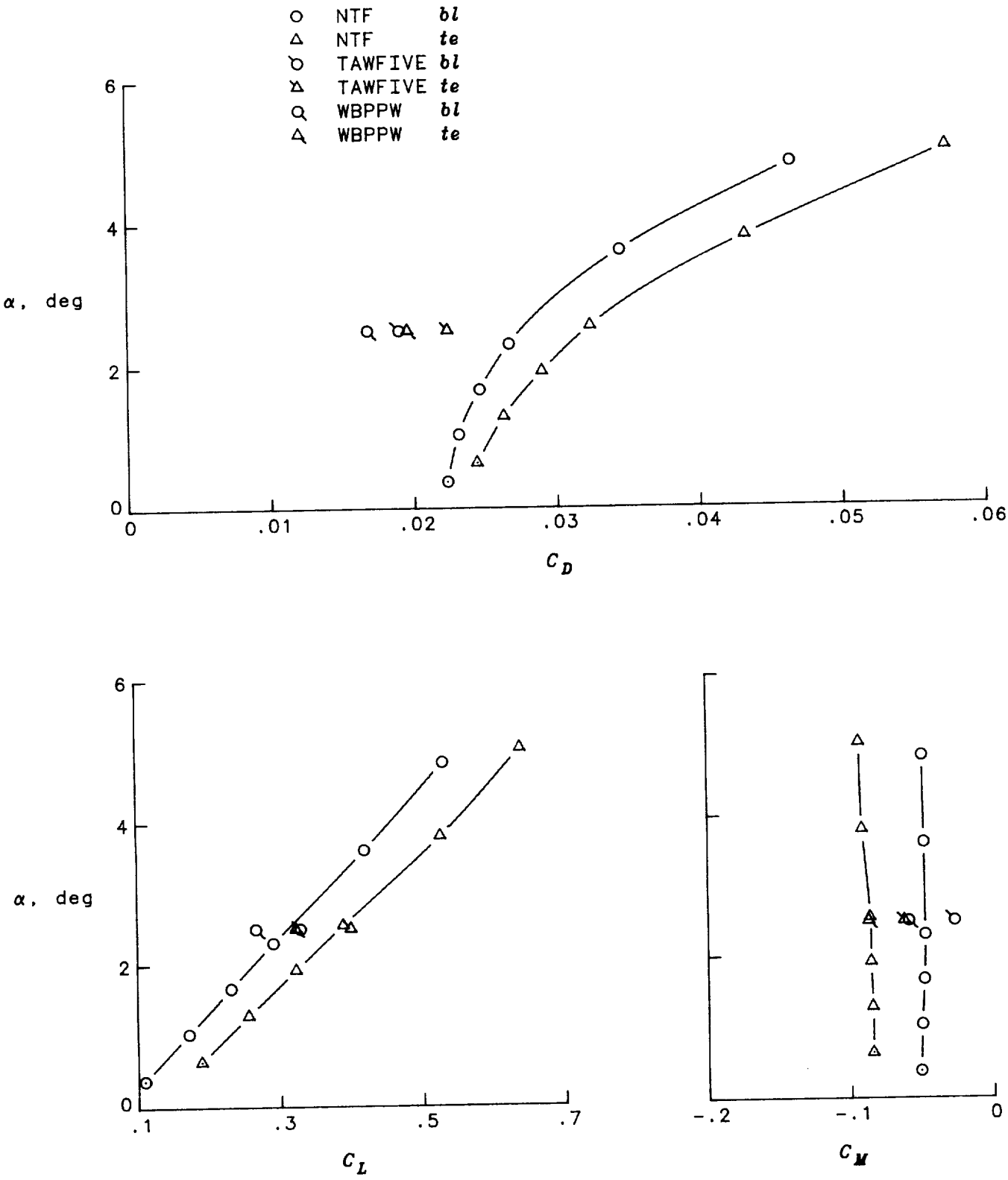

(b) $M = 0.800$.

Figure 13. Concluded.

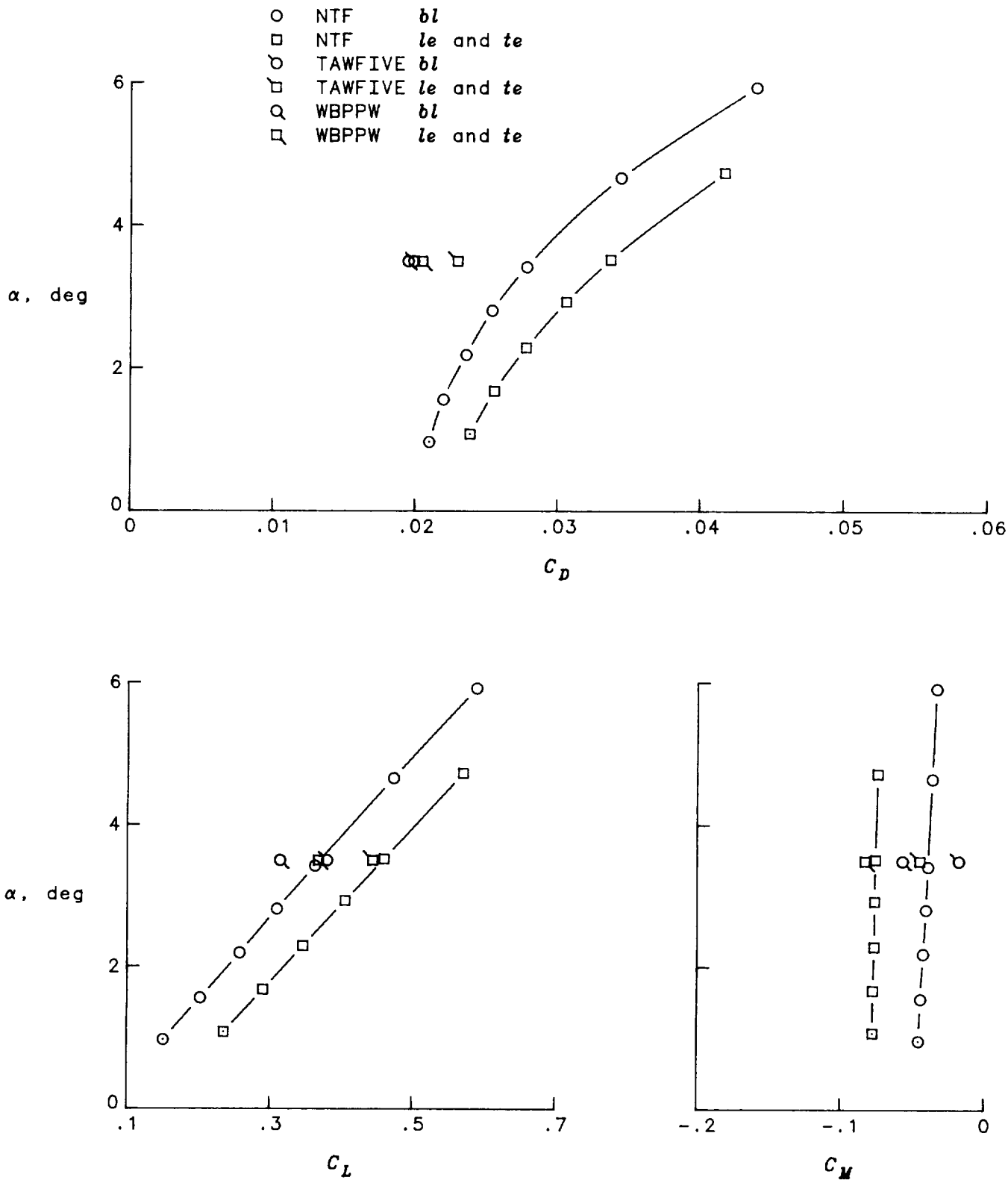

(a) $M = 0.725$.

Figure 14. Comparison of predicted effects of combined modifications with NTF data. $R = 2.7 \times 10^6$.

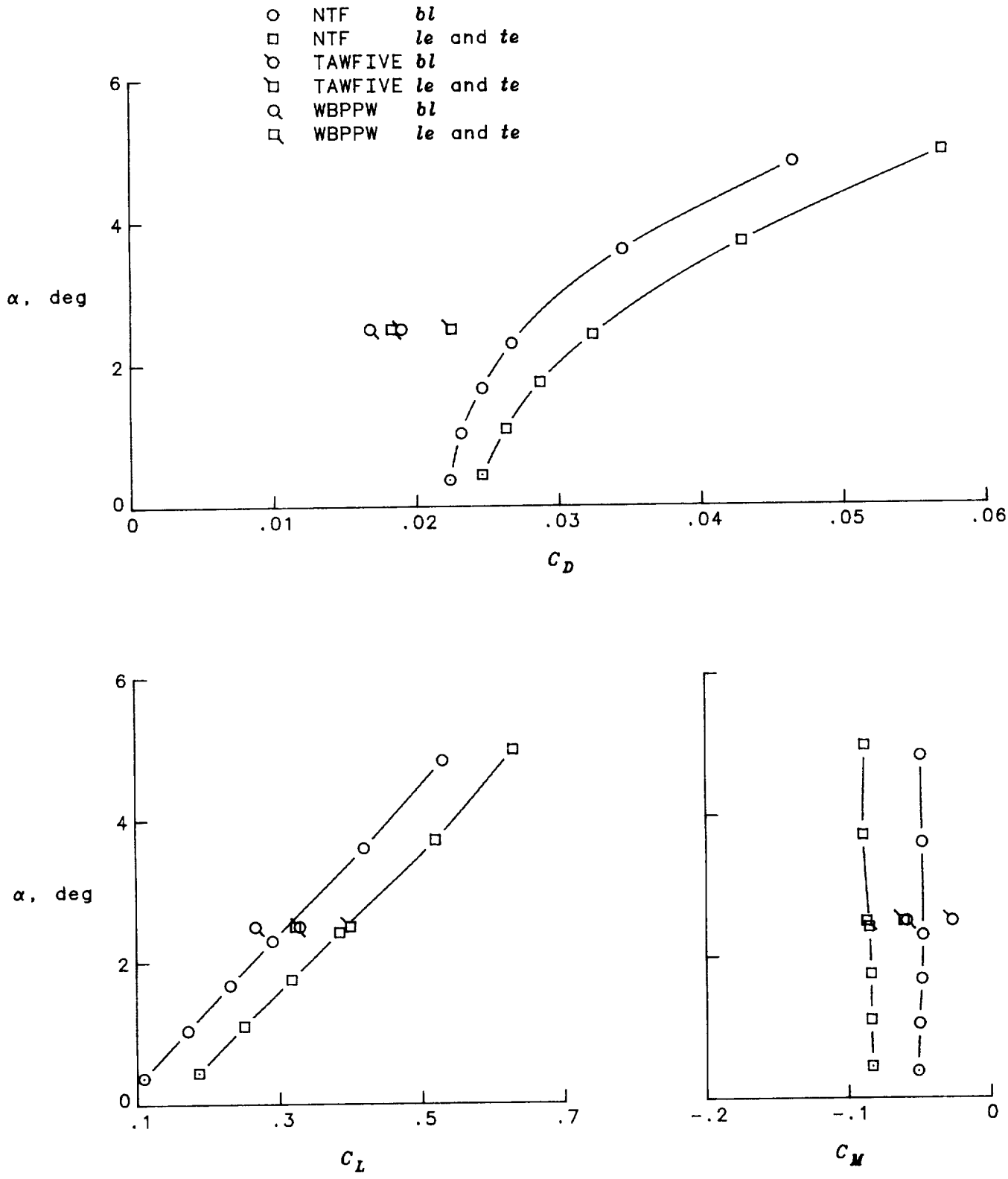

(b) $M = 0.800$.

Figure 14. Concluded.

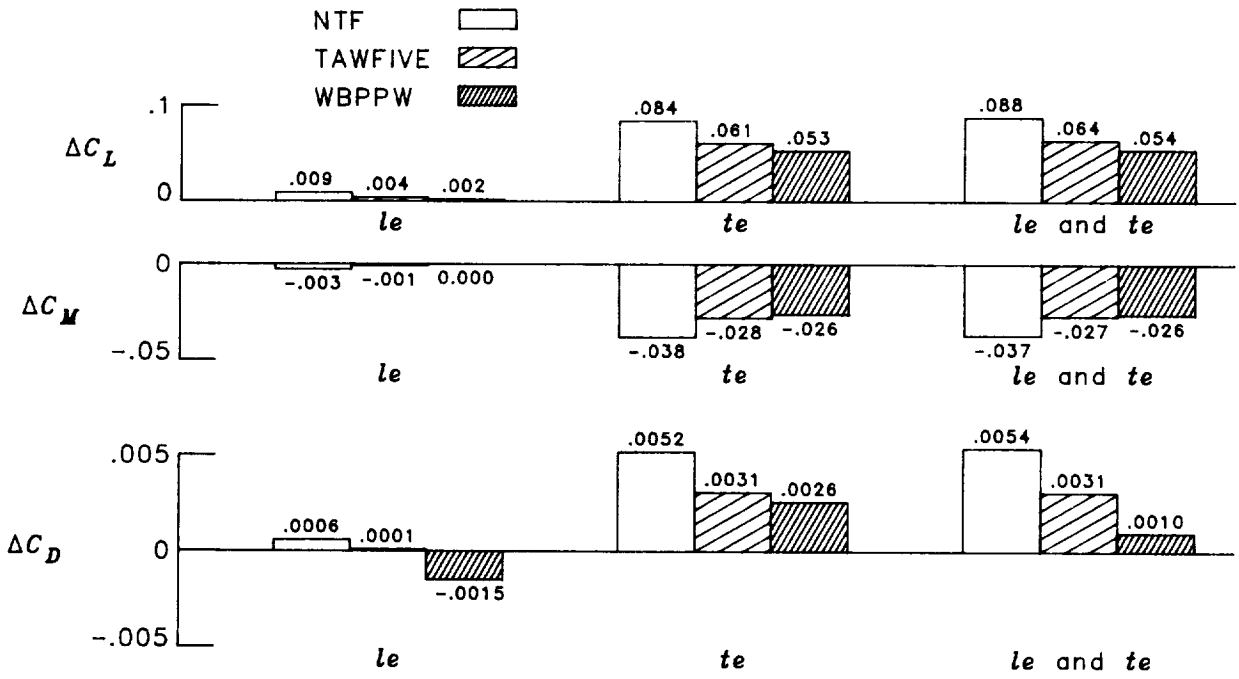

(a) $M = 0.725$, $\alpha = 3.5°$.

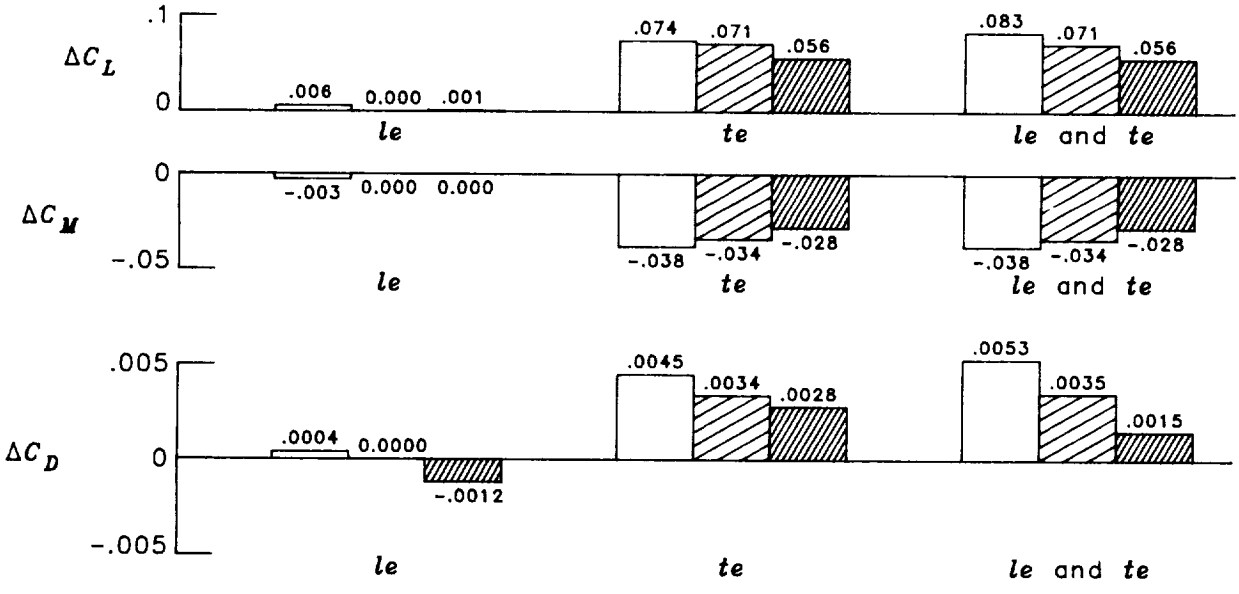

(b) $M = 0.800$, $\alpha = 2.5°$.

Figure 15. Comparison of predicted incremental effects of modified configurations with NTF data. $R = 2.7 \times 10^6$.

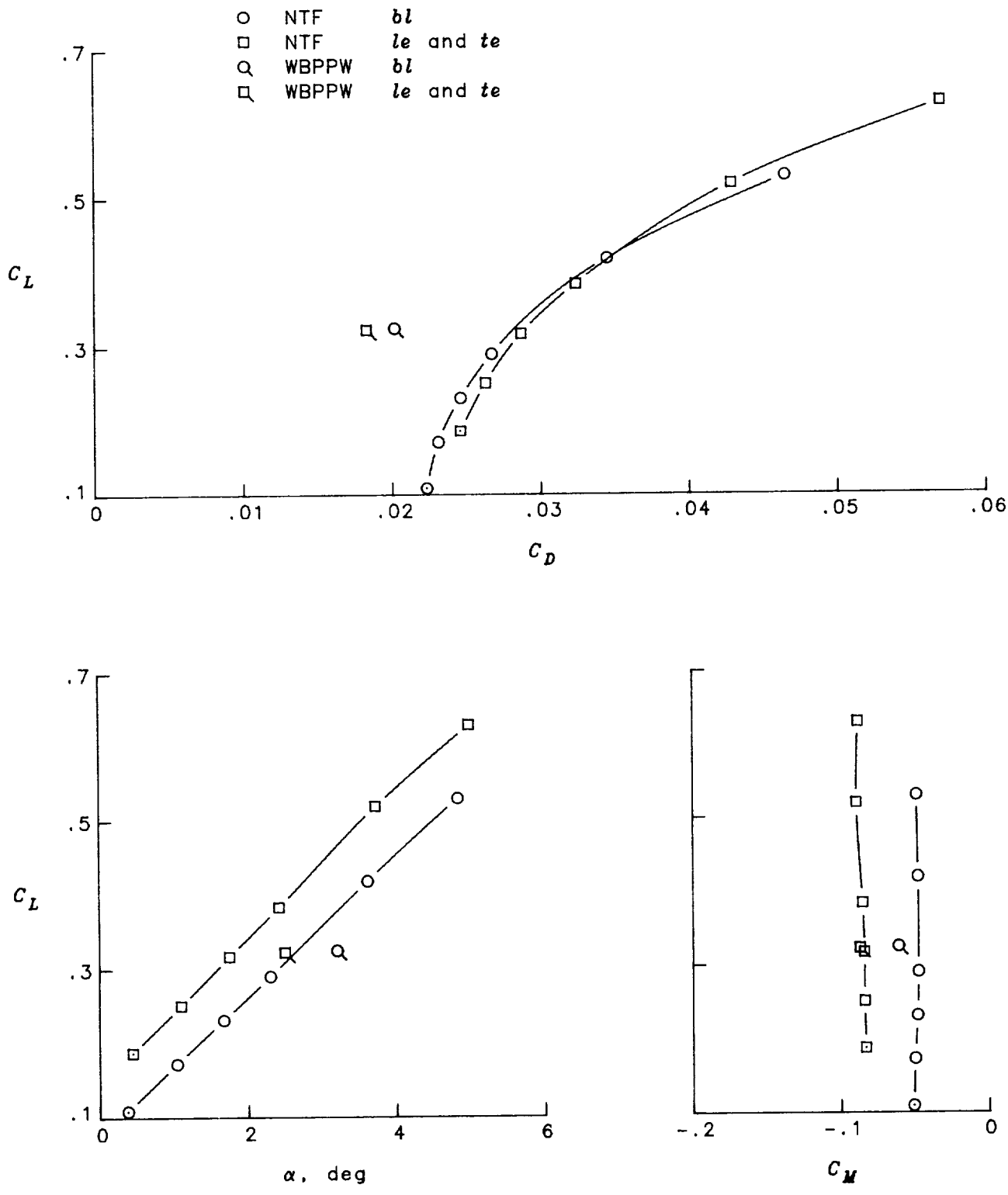

Figure 16. Comparison at common lift coefficient of effects of combined modifications. $M = 0.800$; $R = 2.7 \times 10^6$.

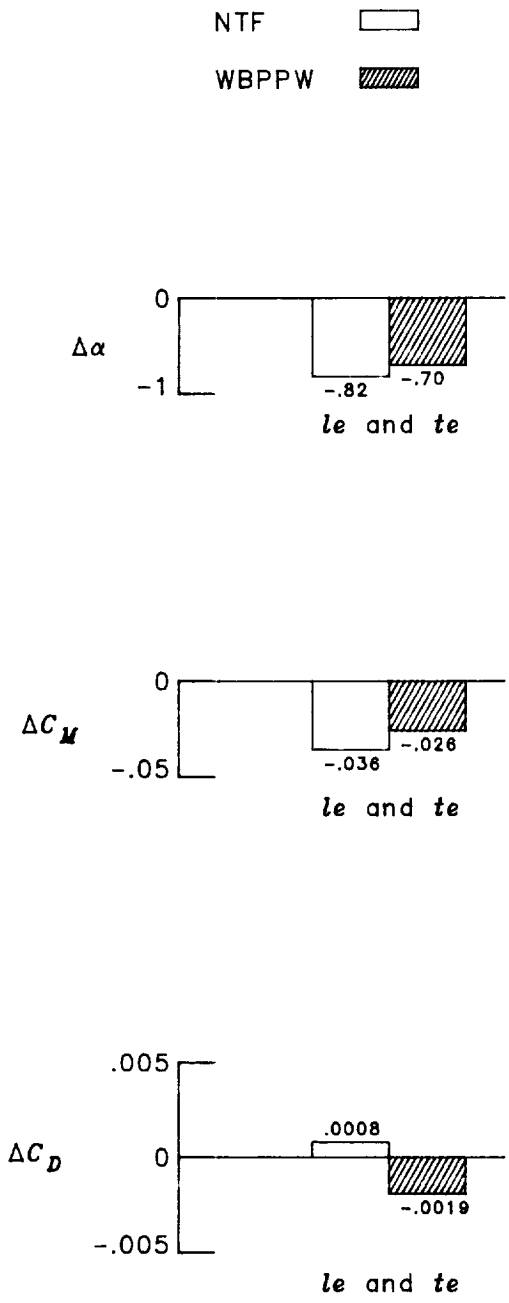

Figure 17. Comparison at common lift coefficient of incremental effects of combined modifications. $C_L = 0.323$; $M = 0.800$; $R = 2.7 \times 10^6$.

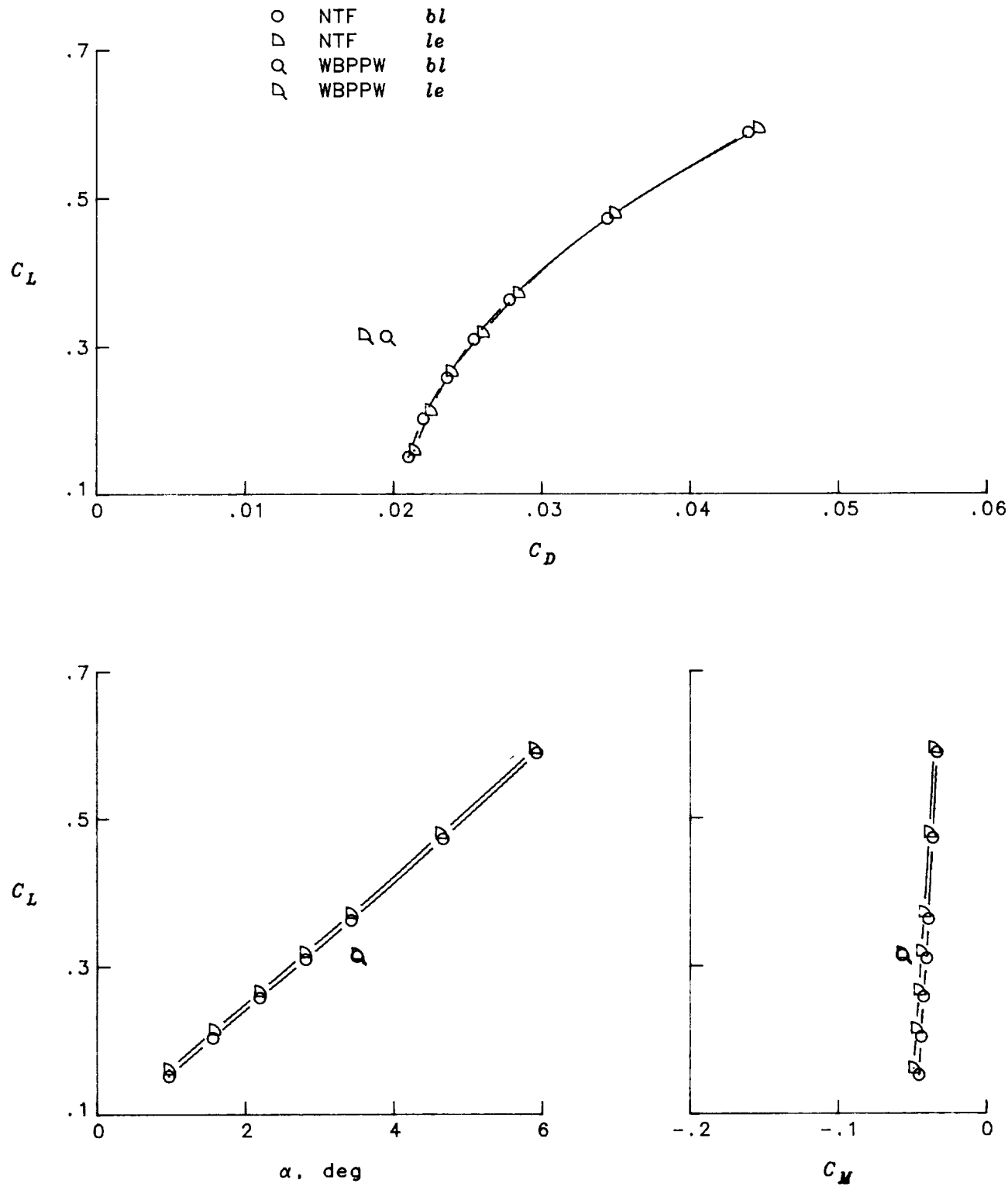

(a) $M = 0.725$.

Figure 18. Lift-matched comparison of effects of leading-edge modification. $R = 2.7 \times 10^6$.

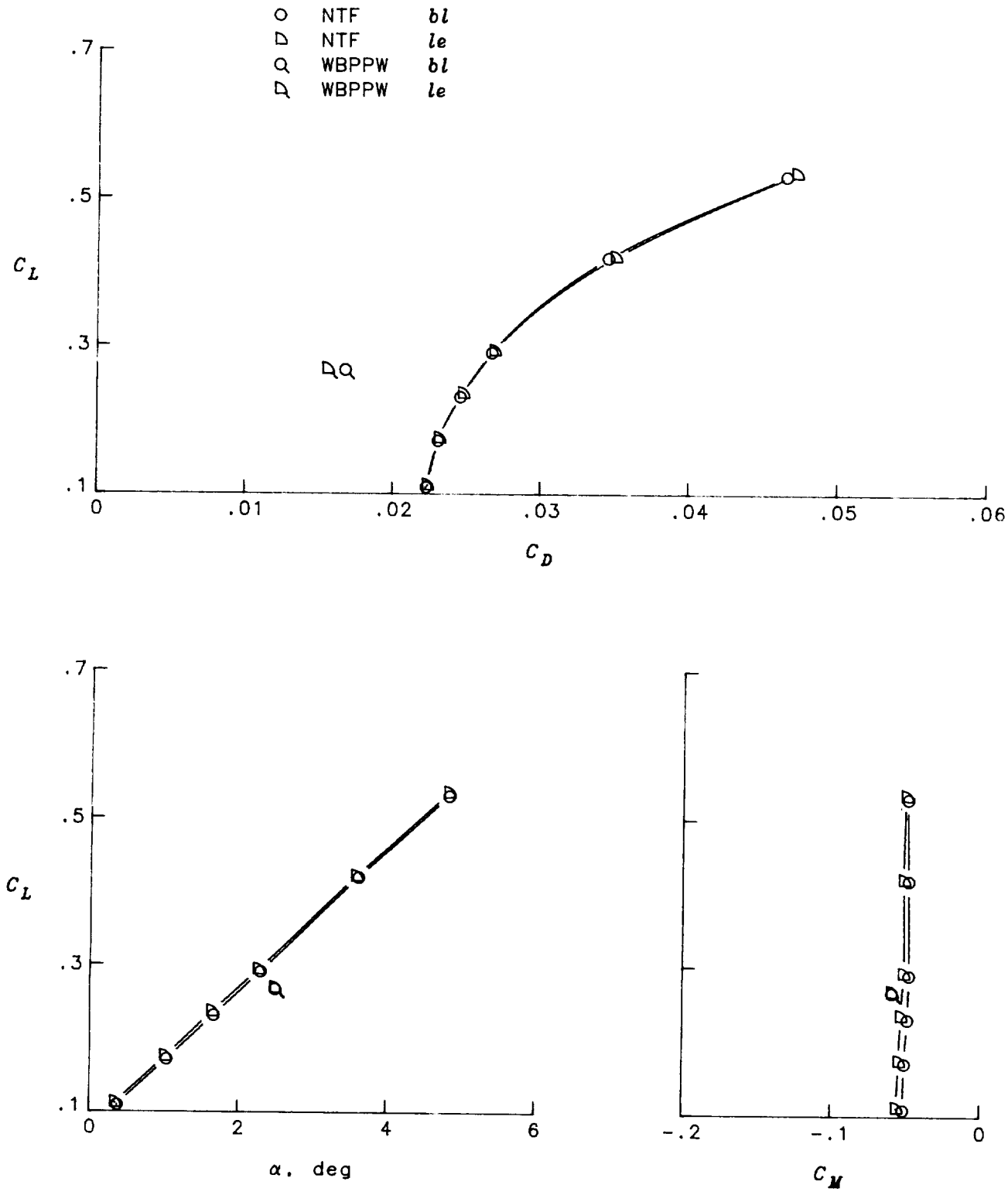

(b) $M = 0.800$.

Figure 18. Concluded.

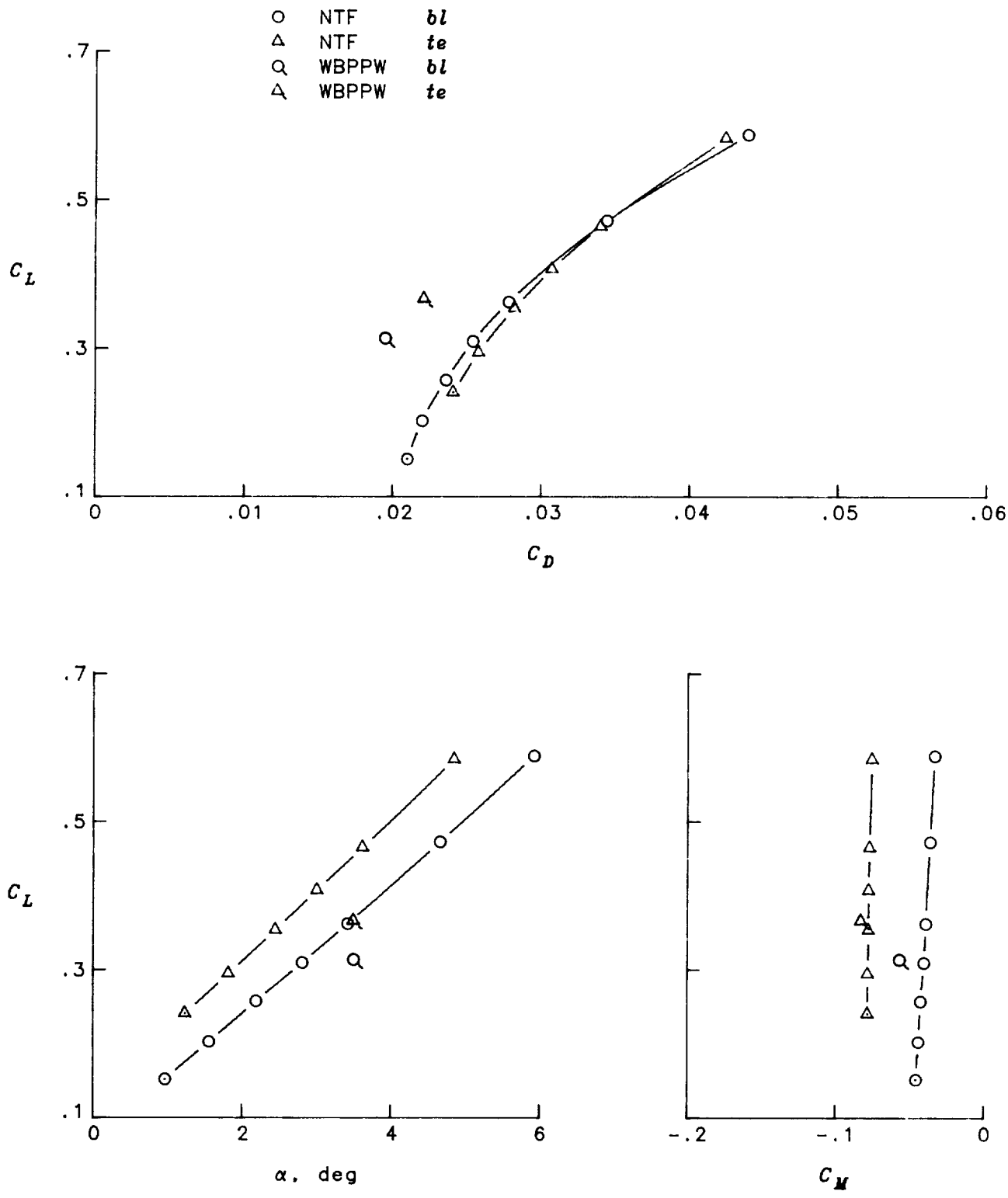

(a) $M = 0.725$.

Figure 19. Lift-matched comparison of effects of trailing-edge modification. $R = 2.7 \times 10^6$.

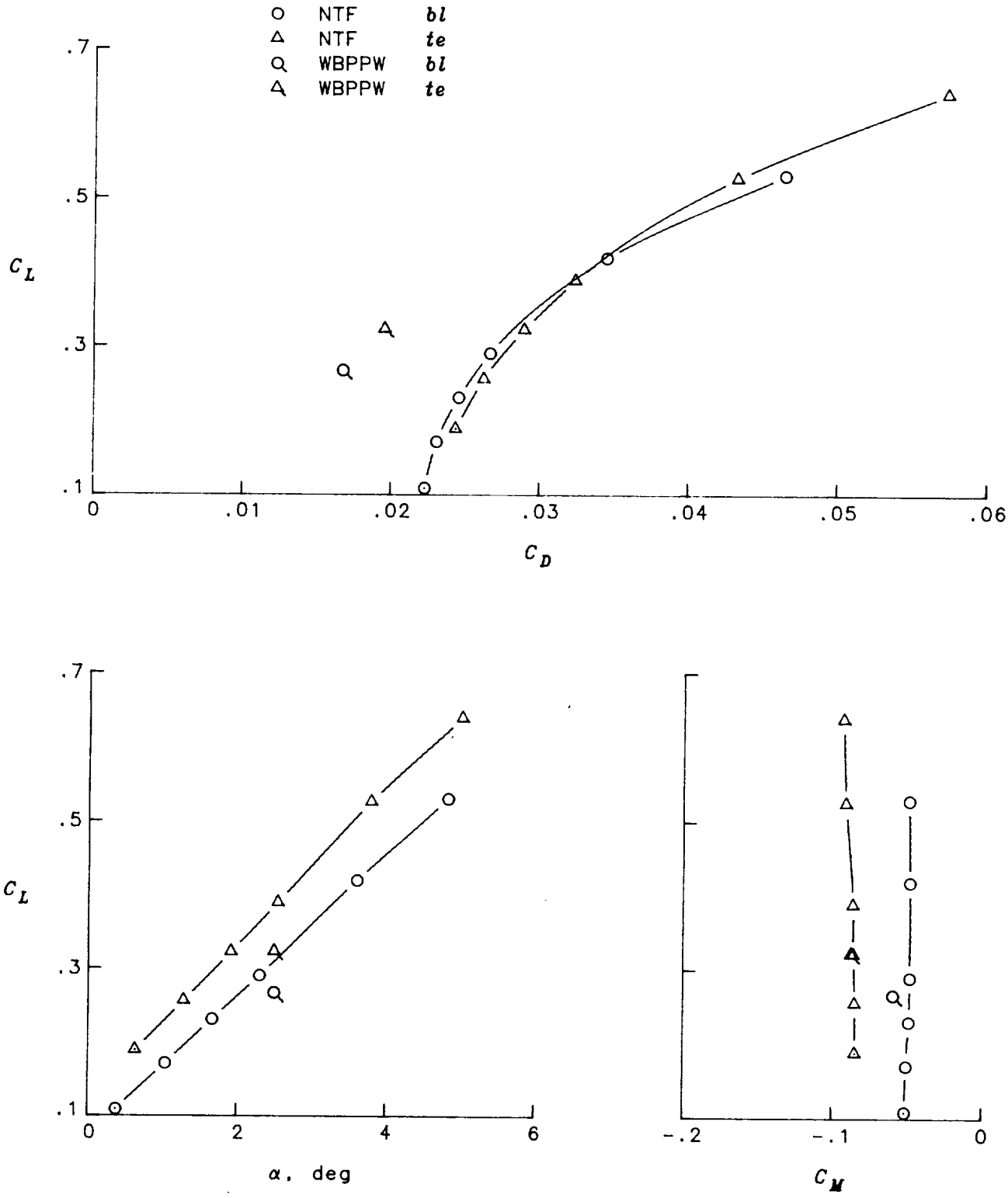

(b) $M = 0.800$.

Figure 19. Concluded.

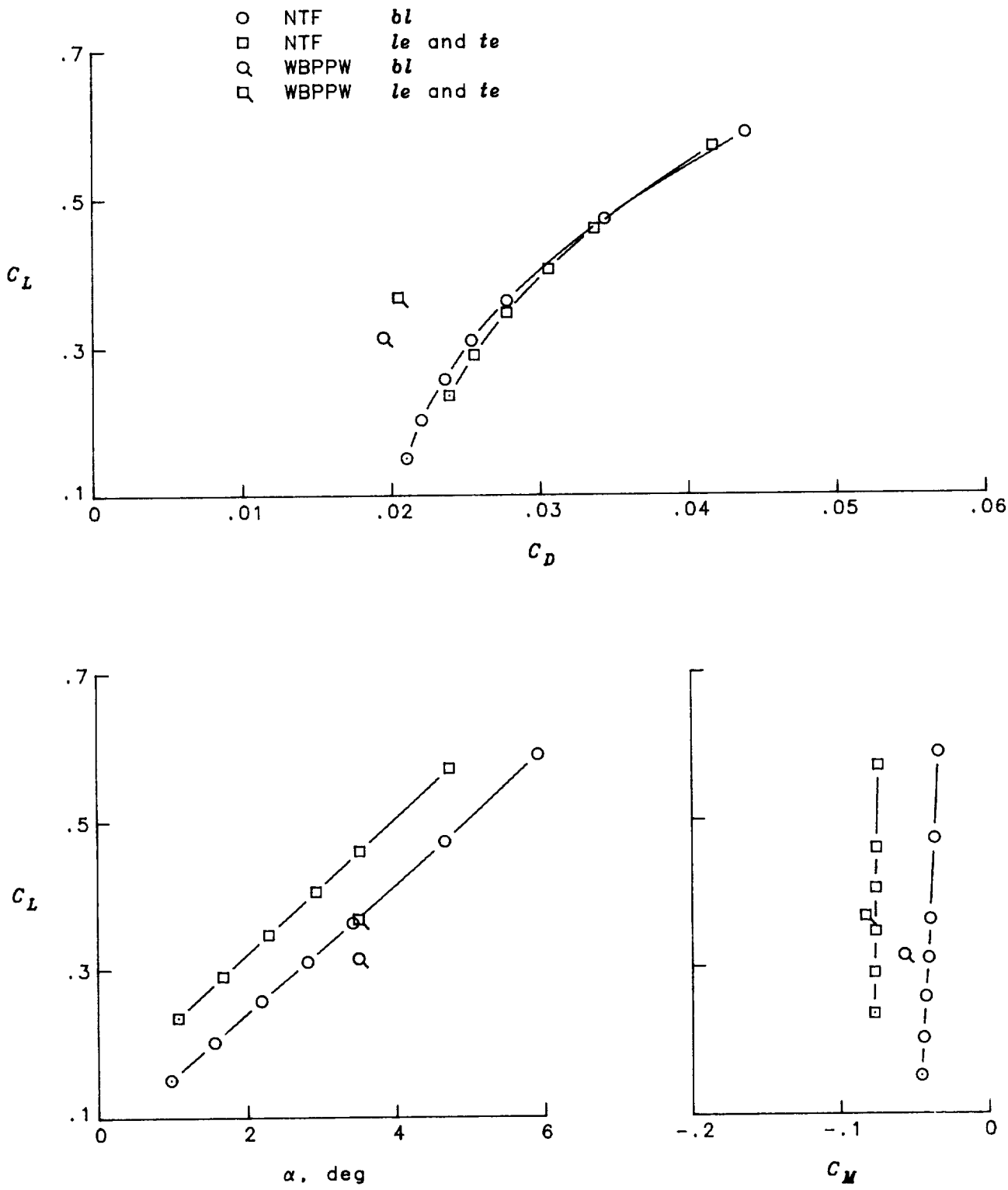

(a) $M = 0.725$.

Figure 20. Lift-matched comparison of effects of combined modifications. $R = 2.7 \times 10^6$.

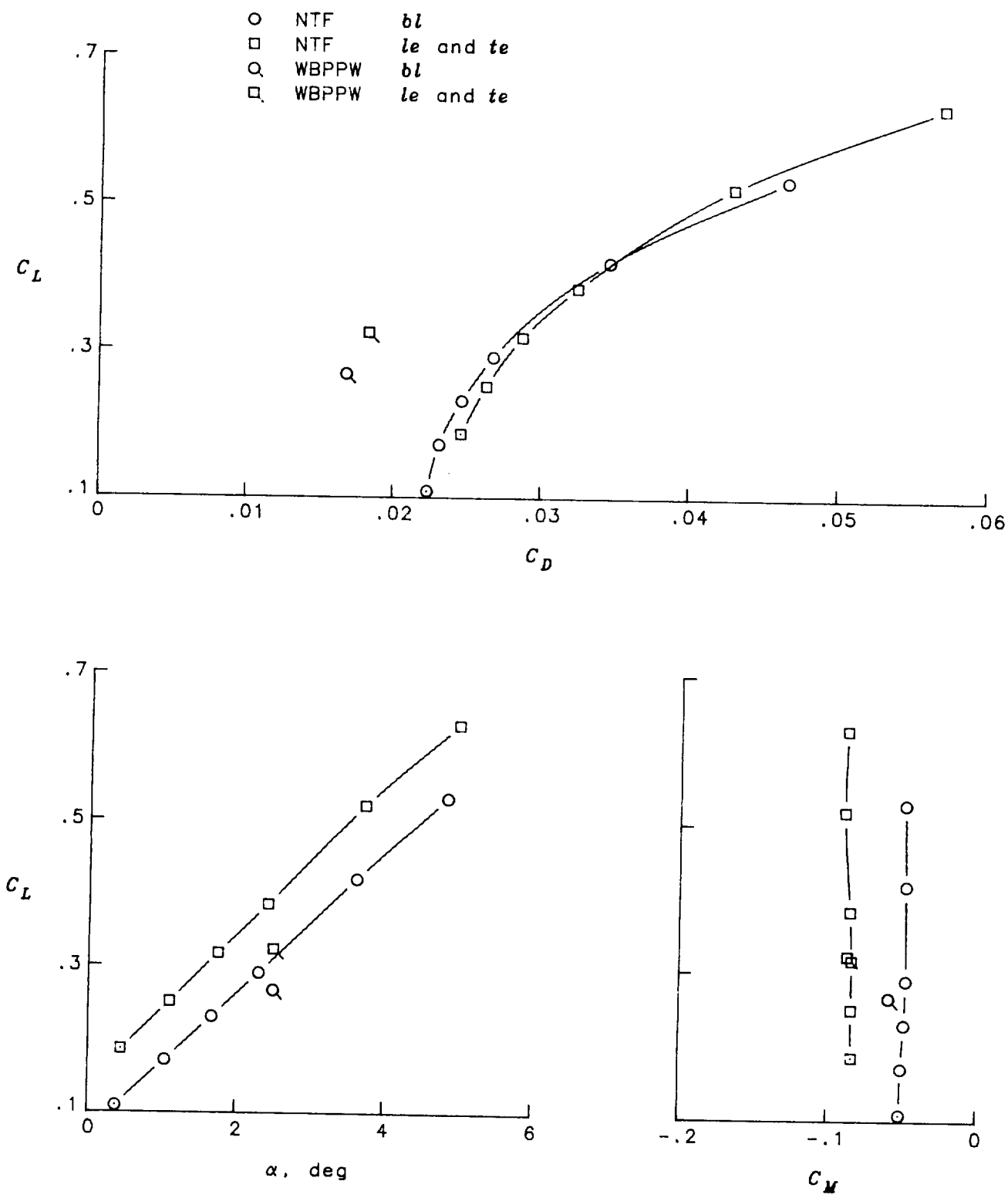

(b) $M = 0.800$.

Figure 20. Concluded.

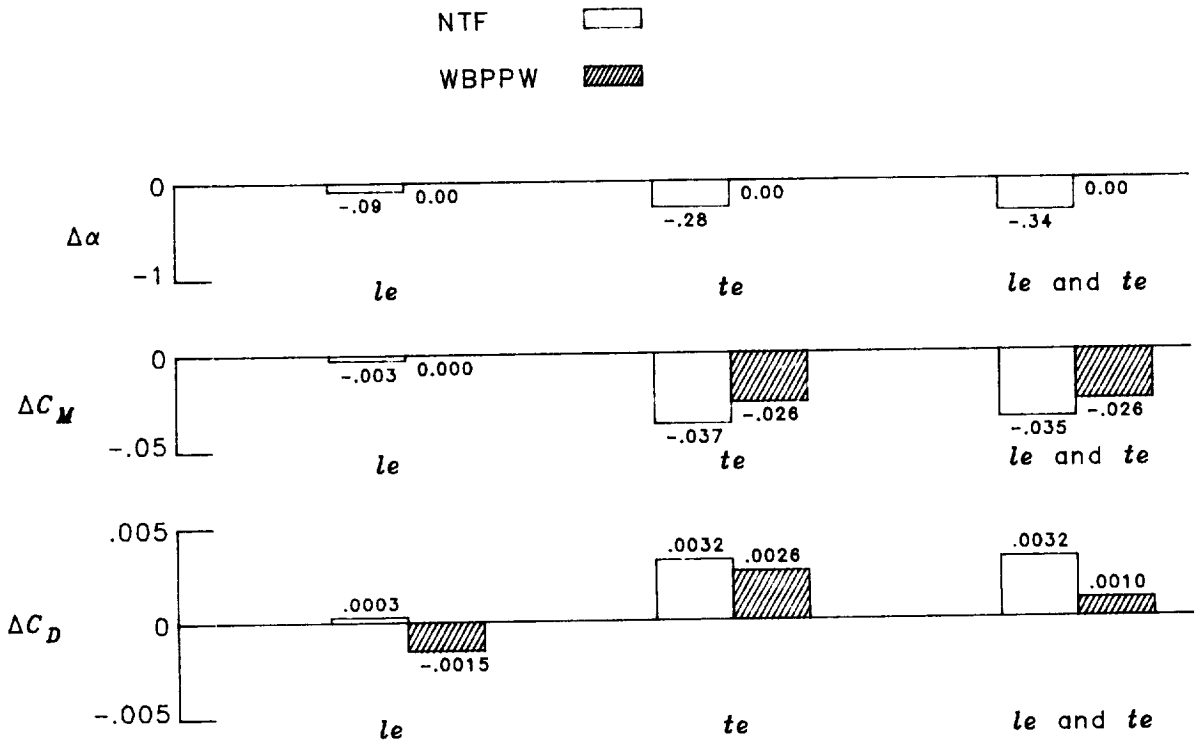

(a) $M = 0.725$.

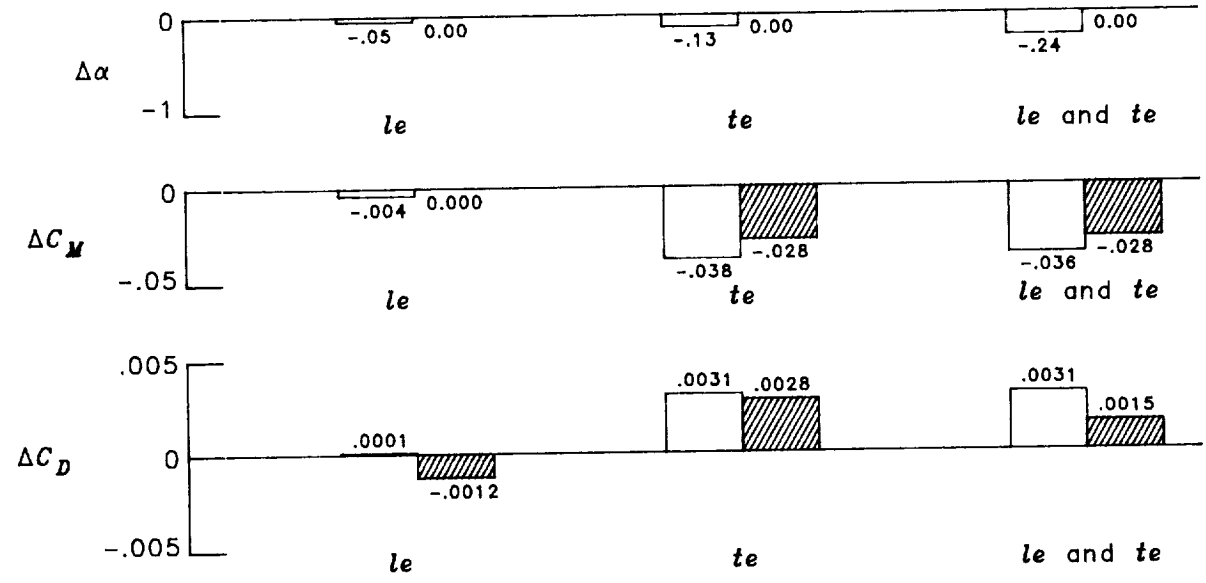

(b) $M = 0.800$.

Figure 21. Lift-matched comparison of incremental effects of modified configurations. $R = 2.7 \times 10^6$.

NASA
National Aeronautics and Space Administration

Report Documentation Page

1. Report No.	2. Government Accession No.	3. Recipient's Catalog No.
NASA TP-3046		

4. Title and Subtitle	5. Report Date
Prediction of Effects of Wing Contour Modifications on Low-Speed Maximum Lift and Transonic Performance for the EA-6B Aircraft	November 1990
	6. Performing Organization Code
7. Author(s)	8. Performing Organization Report No.
Dennis O. Allison and E. G. Waggoner	L-16741
	10. Work Unit No.
9. Performing Organization Name and Address	505-61-21-03
NASA Langley Research Center Hampton, VA 23665-5225	11. Contract or Grant No.
	13. Type of Report and Period Covered
12. Sponsoring Agency Name and Address	Technical Paper
National Aeronautics and Space Administration Washington, DC 20546-0001	14. Sponsoring Agency Code

15. Supplementary Notes

16. Abstract

Computational predictions of the effects of wing contour modifications on maximum lift and transonic performance were made and verified against low-speed and transonic wind-tunnel data. This effort was part of a program to improve the maneuvering capability of the Grumman EA-6B Prowler, an electronics countermeasures aircraft, which evolved from the A-6 Intruder, an attack aircraft. The predictions were based on results from three computer codes that include viscous effects: MCARF, a two-dimensional subsonic panel code; TAWFIVE, a transonic full-potential code; and WBPPW, a transonic, small-disturbance, potential-flow code. The modifications were previously designed with the aid of these and other codes. The wing modifications consist of contour changes to the leading-edge slats and trailing-edge flaps and were designed for increased maximum lift with minimum effect on transonic performance. This report presents the prediction of the effects of the modifications, with emphasis on verification through comparisons with wind-tunnel data from the National Transonic Facility. Attention is focused on increments in low-speed maximum lift and increments in transonic lift, pitching moment, and drag that result from the contour modifications.

17. Key Words (Suggested by Authors(s))	18. Distribution Statement
Computational predictions Contour modifications Incremental effects Maneuver improvement Maximum lift Transonic performance	Unclassified—Unlimited Subject Category 02

19. Security Classif. (of this report)	20. Security Classif. (of this page)	21. No. of Pages	22. Price
Unclassified	Unclassified	45	A03

NASA FORM 1626 OCT 86

NASA-Langley, 1990

For sale by the National Technical Information Service, Springfield, Virginia 22161-2171